NASA TECHNICAL NOTE

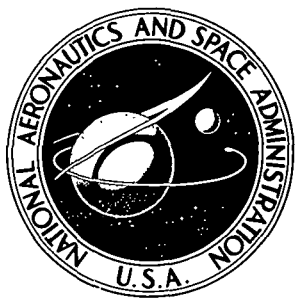

NASA TN D-7302

NASA TN D-7302

FLIGHT RESULTS FROM A STUDY OF AIDED INERTIAL NAVIGATION APPLIED TO LANDING OPERATIONS

by

Leonard A. McGee, Gerald L. Smith, Daniel M. Hegarty, Thomas M. Carson, and Robert B. Merrick

Ames Research Center
Moffett Field, Calif. 94035

S. F. Schmidt and B. Conrad

Analytical Mechanics Associates, Inc.
Mt. View, Calif. 94040

NATIONAL AERONAUTICS AND SPACE ADMINISTRATION • WASHINGTON, D. C. • OCTOBER 1973

1. Report No. NASA TN D-7302	2. Government Accession No.	3. Recipient's Catalog No.
4. Title and Subtitle **FLIGHT RESULTS FROM A STUDY OF AIDED INERTIAL NAVIGATION APPLIED TO LANDING OPERATIONS**		5. Report Date October 1973 6. Performing Organization Code
7. Author(s) Leonard A. McGee, Gerald L. Smith, Daniel M. Hegarty, Thomas M. Carson, and Robert B. Merrick and S. F. Schmidt and B. Conrad		8. Performing Organization Report No. A-4584 10. Work Unit No. 115-17-01-07-00
9. Performing Organization Name and Address NASA Ames Research Center, Moffett Field, Calif. 94035 and Analytical Mechanics Associates, Inc., Mt. View, Calif. 94040		11. Contract or Grant No. 13. Type of Report and Period Covered Technical Note
12. Sponsoring Agency Name and Address National Aeronautics and Space Administration Washington, D. C. 20546		14. Sponsoring Agency Code
15. Supplementary Notes		

16. Abstract

An evaluation is presented of the approach and landing performance of a Kalman filter aided inertial navigation system using flight data obtained from a series of approaches and landings of the Ames CV-340 aircraft at an instrumented test area of the White Sands Missile Range (WSMR). A description of the flight test is given, in which data recorded included: (1) accelerometer signals from the platform of an INS; (2) three ranges from the Ames-Cubic Precision Ranging System; and (3) radar and barometric altimeter signals. The method of system evaluation employed was postflight processing of the recorded data using a Kalman filter which was designed for use on the XDS920 computer onboard the CV-340 aircraft. Results shown include comparisons between the trajectories as estimated by the Kalman filter aided system and as determined from WSMR cinetheodolite data. "Data start" initialization of the Kalman filter, operation at a practical data rate, postflight modeling of sensor errors and operation under the adverse condition of bad data are illustrated.

17. Key Words (Suggested by Author(s)) Airborne aided inertial navigation system, Kalman filter (square-root formulation), radar and barometric altimeters, cinetheodolite tracking.	18. Distribution Statement Unclassified – Unlimited		
19. Security Classif. (of this report) Unclassified	20. Security Classif. (of this page) Unclassified	21. No. of Pages 44	22. Price* Domestic, $3.00 Foreign, $5.50

*For sale by the National Technical Information Service, Springfield, Virginia 22151

Page Intentionally Left Blank

TABLE OF CONTENTS

Page Intentionally Left Blank

SYMBOLS

A_0, A_1, A_2	constants representing position, velocity, and acceleration, respectively, in least-squares solution
B_1, B_2, B_3	bias values for subscript ACPRS range calibration
C_i	coefficients determined from the principle matrix in a least-squares solution (i = X, Y, Z, $\dot{X}$, $\dot{Y}$, $\dot{Z}$)
K_1, K_2, K_3	scaling constants for subscript ACPRS range calibration
ΔM	measurement residual
N	number of time points in a least-squares fit
q	computed standard deviation of the measurement residual, ΔM
R_1, R_2, R_3	measured ranges from ACPRS subscript transponder to aircraft antenna
$\dot{R}_1, \dot{R}_2, \dot{R}_3$	range-rates to subscript ACPRS transponder
$\Delta R_1, \Delta R_2, \Delta R_3$	differences between measured and WSMR computed range to subscript transponder
ΔR_c	range calibration correction computed at time of range measurement
S_A^2	sample angular variance
S_i^2	sample variance of ith state component (i = X, Y, Z)
$\Delta V_x, \Delta V_x, \Delta V_y$	changes in subscripted velocity due to integration of acceleration over a fixed time interval (output from Electronic Interface Unit)
X,Y,Z	aircraft positions (position of LTN-51 INS) in the Runway Coordinate System
$\dot{X}, \dot{Y}, \dot{Z}$	aircraft velocities (velocity of LTN-51 INS) in the Runway Coordinate System
$\bar{X}, \bar{Y}, \bar{Z}$	position coordinates determined from cinetheodolite angle data
Z_{oi}, X_{oi}, Y_{oi}	locations of the ith transponder antenna in the Runway Coordinate System (i = 1, 2, 3)
$\hat{\sigma}_i$	WSMR estimate of the standard deviation in the ith state component (i = X, Y, Z, $\dot{X}$, $\dot{Y}$, $\dot{Z}$)

GLOSSARY

ACPRS	Ames Cubic Precision Ranging System
AGC	Automatic Gain Control
ARC	Ames Research Center (NASA)
ARINC	Aeronautical Radio, Inc. (Conforms to standards and format specified by Aeronautical Radio, Inc.)
ARP	Aircraft Reference Point
CTOL	Conventional Takeoff and Landing
EIU	Electronic Interface Unit
ILS	Instrument Landing System
IMU	Inertial Measurement Unit
INS	Inertial Navigation System
MLS	Microwave Landing System
MSC	Manned Spacecraft Center, NASA (now JSC, Johnson Spacecraft Center)
NAVAID	Navigation Aid (e.g., TACAN)
RAINPAL	Recursive Aided Inertial Navigation for Precision Approach and Landing
SSV	Space Shuttle Vehicle
TACAN	Tactical Air Navigation – a military omnibearing and distance-measuring system
UHF	Ultrahigh Frequency
VORTAC	A combined civil omnibearing and military distance-measuring system
V/STOL	Vertical/Short Takeoff and Landing
WSMR	White Sands Missile Range

FLIGHT RESULTS FROM A STUDY OF AIDED INERTIAL NAVIGATION APPLIED TO LANDING OPERATIONS

L. A. McGee, G. L. Smith, D. M. Hegarty,
T. M. Carson, and R. B. Merrick

Ames Research Center

and

S. F. Schmidt and B. Conrad

Analytical Mechanics Associates, Inc.

SUMMARY

An evaluation is presented of the approach and landing performance of a Kalman filter aided inertial navigation system using flight data obtained from a series of approaches and landings of the Ames CV-340 aircraft at an instrumented test area of the White Sands Missile Range (WSMR). A description of the flight tests and the test apparatus is given, in which data recorded onboard the aircraft included (1) accelerometer signals from the platform of an Inertial Navigation System (INS), (2) three ranges from the Ames/Cubic Precision Ranging System (ACPRS), (3) radar and barometric altimeter signals, and (4) time.

The recorded data were processed postflight to provide an estimated trajectory of the aircraft during the flight test. The data processing computer software used a Kalman filter and was designed to operate onboard the CV-340 aircraft in real time or postflight in a ground-based facility. This software is described, including the techniques used for rejecting "bad data" and for initializing the Kalman filter from in-flight data measurements. Typical results of the filter initialization are given.

Error models for the recorded data are presented along with an expression for in-flight calibration of the ranges for anomalous behavior discovered in the Ames Cubic Precision Ranging System.

The performance of the WSMR cinetheodolite tracking system was analyzed for the situation in which the aircraft was stationary at a known location on the ground after each landing. Certain results of this analysis carry over to the situation in which the aircraft is in flight.

The flight-test results were based primarily on comparisons between the trajectories estimated by the aided inertial system and that determined by the cinetheodolite data. The test results compare position and velocity components with emphasis on the final 40 seconds before touchdown.

Among the more important conclusions reached was that the aided inertial system is capable of navigation accuracies sufficient to meet very stringent automatic landing requirements. These accuracies also qualify the system as an independent reference against which other navigation systems could be evaluated. In applications where the reference system can be carried onboard the test vehicle, this approach would have outstanding advantages over a cinetheodolite reference system. Another significant conclusion, particularly for onboard applications, is that an effective square-root form of the

Kalman filter was demonstrated which includes an efficient method for modeling random forcing functions.

INTRODUCTION

Accurate and reliable navigation systems will play a vital role in aircraft operations of the future. The most critical role will be to provide essential information to an automatic landing system. Recent trends clearly show that the airline industry is moving steadily toward the use of automatic landing systems. The Space Shuttle Vehicle (SSV), designed to land without engine power, must have a very sophisticated automatic landing system. These examples show there is a growing need to develop navigation concepts that will keep pace with the increasing demands being placed on automatic landing system technology.

The flight-test results presented here are the outcome of a joint program between NASA's Ames Research Center (ARC) and Manned Spacecraft Center (MSC) and the Army's Instrumentation Directorate at the White Sands Missile Range (WSMR-ID) to study a particular navigation concept with emphasis on approach and landing. These studies evolved from (1) an ARC desire to test a Kalman filter aided inertial navigation system called RAINPAL (Recursive Aided Inertial Navigation for Precision Approach and Landing) that has wide application in many types of aircraft such as V/STOL and CTOL, (2) an MSC desire to investigate new concepts suitable for navigation of the SSV during approach and landing, and (3) a WSMR-ID desire to investigate new concepts that offer promise as a future instrumentation system for the WSMR.

The RAINPAL system uses a square-root form of the Kalman filter to process data received from ground navigation aids and from onboard altimeter measurements to update an Inertial Navigation System (INS). While a variety of ground navigation aid data can be used, this test used three ranges from the aircraft to transponders on the ground as measured by the Ames Cubic Precision Range System (ACPRS). When operated in conjunction with a barometric or radar altimeter, this concept (as shown by extensive simulation studies, refs. 1-3) can provide precision navigation during approach and landing.

Most Kalman filter updating systems that have operated in the recent past (ref. 4) have used conventional filter formulations. The square-root formulation was initially developed for use with small computers that have difficulty retaining sufficient accuracy without resorting to extremely time-consuming "extra precision." Random forcing functions were not used for dynamic model error compensation in these early filters since techniques for including such effects required prohibitive calculation times and/or computer storage. Recent advances (refs. 5 and 6) in computational techniques have resulted in efficient methods for adding the random forcing functions that make the square-root formulation highly attractive for airborne use. Capitalizing on these advances, a major objective of this test program was to demonstrate such a Kalman filter in an airborne aided inertial system.

An extensive fixed-point software program was developed for the XDS-920 computer onboard the CV-340 which would allow in-flight, real-time operation of the RAINPAL system (ref. 7) or in-flight data recording for later processing. This same software also allowed postflight processing of the in-flight recorded data on a XDS-920 computer located in a laboratory. This postflight data analysis facility proved invaluable in developing and validating the onboard RAINPAL mechanization.

To validate the navigation performance of the real-time RAINPAL system, a series of flight tests was conducted at the White Sands Missile Range (WSMR). System performance was measured during approach and landing by comparing the aircraft position and velocity measurements obtained from the WSMR cinetheodolite tracking data with those computed by the RAINPAL system. The comparisons presented here are restricted to 130 seconds before touchdown (beginning of glideslope) with major emphasis on the final 40 seconds before touchdown.

The authors gratefully acknowledge their indebtedness to the many persons who contributed considerable time and effort to the planning, preparation, data handling, and conduction of the flight tests at White Sands Missile Range. These persons, listed alphabetically by agency, are:

NASA/ARC:

Frederick G. Edwards
Gordon H. Hardy
Henry C. Lessing
Milo D. Reisner
Gilbert G. Robinson
Glen W. Stinnett, Jr.

NASA/MSC:

J. T. Chapman
Ronald C. Epps
Ellis W. Henry
Carl F. Koontz
William A. Middleton
J. Bruce Williamson

White Sands Test Facility:

George M. Ortiz

U. S. Army (Instrumentation Directorate, White Sands Missile Range):

J. F. Hernandez

TEST SITE AND APPARATUS

Test Site

The test site was a dry lake bed near the north end of Northrup Strip at the White Sands Missile Range. A takeoff and landing strip had been graded and rolled just before the flight tests began. Nineteen sites, surveyed to an accuracy of ±7.6 cm (±3 in.), were located on and near the strip. Site 1 was designated as the origin of the runway coordinate system. Figure 1 is a diagram of the test area showing the positive directions of the runway coordinate system (tangent to the earth's surface at site 1) and the three sites where ACPRS transponders were deployed. The remaining surveyed sites were used for other parts of the flight tests.

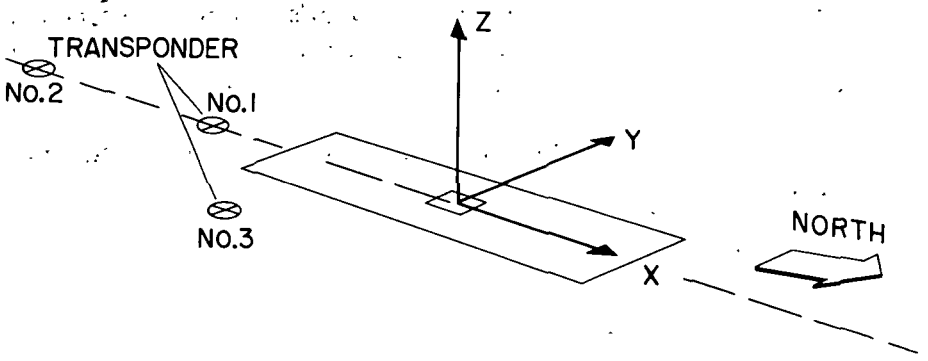

Figure 1. – Test site at Northrup Strip.

Test Aircraft and Airborne Apparatus

The test aircraft was the ARC CV-340 shown in figure 2. This figure gives some of the basic aircraft characteristics and shows a cutaway view of the cabin interior and the radome exposing some of the test airborne apparatus. The test airborne apparatus consisted of (1) an XDS-920 (formerly SDS 920) digital computer, (2) the ACPRS precision ranging system, (3) time-code generator, (4) LTN-51

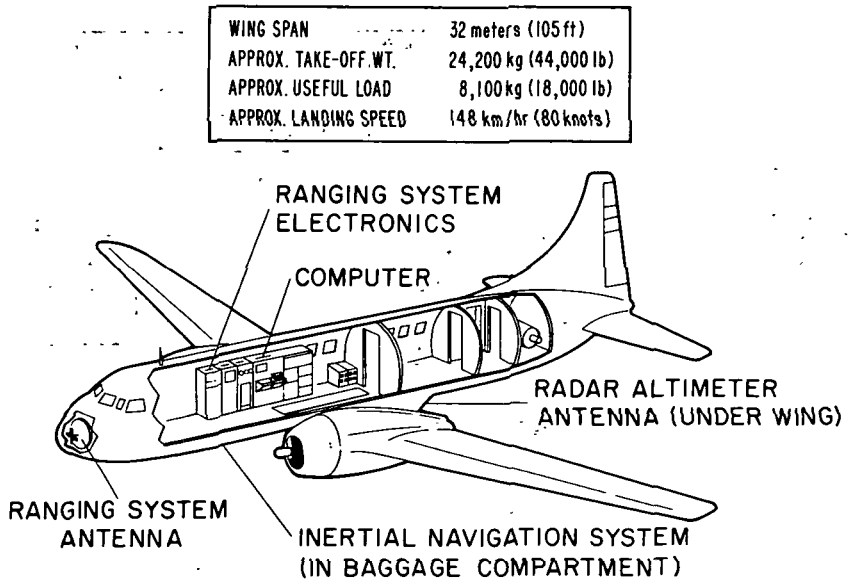

Figure 2. – CV-340 test aircraft.

INS and the associated Electronic Interface Unit (EIU), and (5) barometric and radar altimeters. To aid in understanding later discussions, some elaboration of certain aspects of the onboard apparatus is necessary. The XDS-920 computer is a general purpose machine repackaged for aircraft operation. It has a 12K word memory and a word length of 24 bits including the sign. The ACPRS precision range system measures simultaneously the range from the aircraft to each of the three ground transponders. Reference 8 gives the maximum unambiguous range as approximately 56 km (30 n.mi.) and the range resolution as 21.4 cm (0.7 ft). The onboard transmitter and the ground transponders operate in the 262 to 310 MHz band. The Litton LTN-51 INS and the EIU were next to each other in the baggage compartment beneath the floor of the forward cabin. The LTN-51 is the reference point on the aircraft to which all position and velocity data in this report are referenced and to which all WSMR tracking data were ultimately referred. The barometric altimeter is a Rosemount Engineering Co. Model 840E-2F. Located in a rack behind the copilot's seat, it was attached to the aircraft pitot-static system but was completely independent of the cockpit altimeters in every other respect. There was no feature for manually inserting a correction for local atmospheric pressure.

Figure 3 is a block diagram showing the interconnection of the onboard equipment. For these tests, the following quantities were recorded:

(1) three ranges from the ACPRS

(2) radar and barometric altitudes

(3) ΔV_x, ΔV_y, and ΔV_z (changes in velocity along LTN-51 platform axes)

(4) LTN-51 platform gimbal angles

(5) latitude, longitude, north-south velocity, east-west velocity, and true heading from the LTN-51 ARINC data bus

(6) time to nearest millisecond

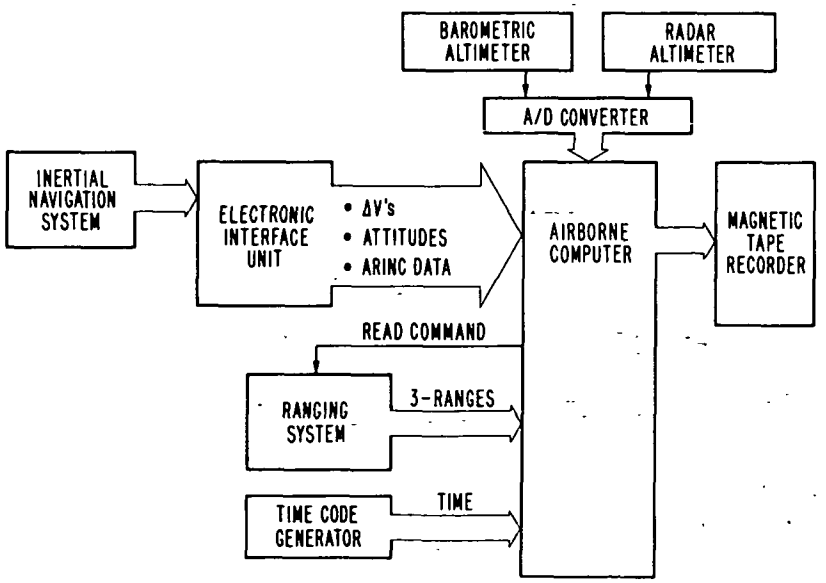

Figure 3. – Block diagram of flight-test equipment.

The inertial data, ΔV_X, ΔV_Y, and ΔV_Z, were obtained from a Litton LTN-51 Inertial Navigation System (INS) in the form of analog X, Y, and Z acceleration signals. A special interface (EIU) was designed and constructed which would simultaneously integrate these accelerometer signals and convert them into 12-bit digital delta-velocity words. These words were placed into holding registers in the EIU to await parallel transfer into the XDS-920 computer. Placement of the delta-velocity words into holding registers was initiated by a high-priority interrupt signal that also caused the computer to immediately transfer these words into its memory. This high-priority interrupt signal was precisely controlled at a frequency of once every 65.911 msec (approximately 16 times per second). A second signal, synchronized with the high-priority interrupt signal and 1/4 its frequency, was used to control the sampling of all navigation aid data, to time-tag the data, and to record all the data on magnetic tape. (All measurements and computations were carried out in the English system of units.)

ACPRS Transponders

An ACPRS transponder is shown in figure 4. The transponder with its associated antenna is shown mounted atop a surveyor's tripod. The overall height of the tripod-transponder-antenna combination is approximately 254 cm (100 in.). The transponder itself weighs about 9 kg (20 lb) and is normally powered by a battery pack located on the ground. Before the WSMR flight tests, the factors influencing the placement of transponders (refs. 1-3) were investigated. From these studies, it was shown that:

(1) Locating two properly spaced transponders directly under the approach path would enable the system to obtain accurate estimates of the barometric altimeter bias as the aircraft passed overhead.

(2) At least one transponder must be placed to the side of the runway to provide good cross-runway (Y) information at touchdown.

Flight tests of the ACPRS system were conducted to determine whether data from the ACPRS were obtainable in a direct overflight at altitudes as low as 12.2 m (40 ft). The results showed that data were available until shortly after the aircraft had passed overhead. This data dropout is due to the restricted ACPRS antenna pattern. With the antenna in the nose of the CV-340, the antenna pattern effectively covers only the forward hemisphere. Based on this flight-test data and on the simulation results, the ACPRS transponders were located at the three surveyed sites shown in figure 1. The transponder antenna coordinates in the runway coordinate system are given in table 1.

TABLE 1.– TRANSPONDER ANTENNA COORDINATES

Transponder no.	Antenna coordinates (X, Y, Z), m (ft)
1	-2,745.19, 0.04, 0.59 (-9,000.61, 0.12, 1.93)
2	-5,795.27, 0.06, -2.02 (-19,000.90, 0.20, -6.61)
3	-914.78, -915.21, 2.23 (-2,999.27, -3000.70, 7.32)

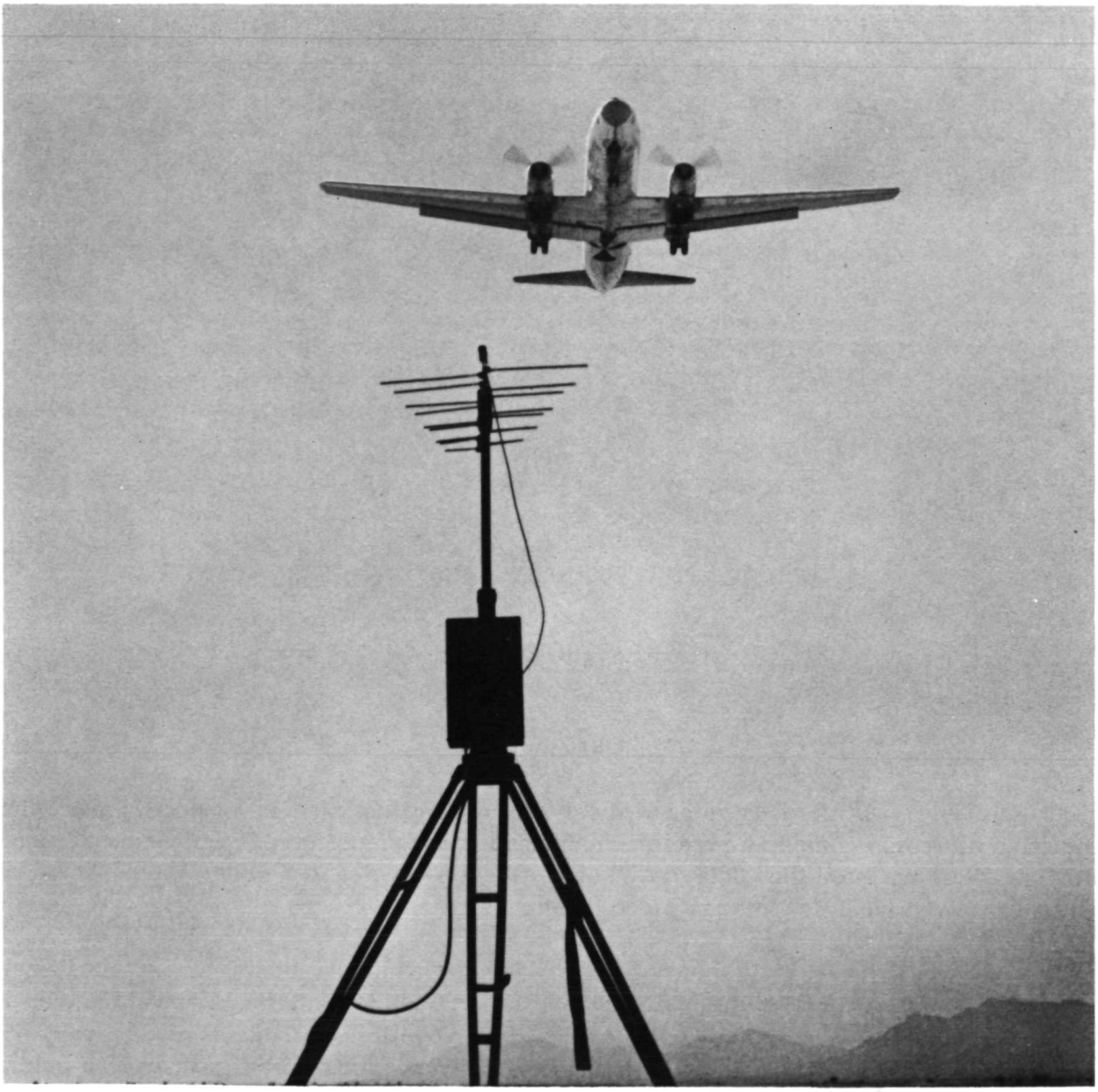

Figure 4.– ACPRS ground transponder.

Flight Pattern

The flight-test data described in this report were obtained by flying a series of three "racetrack" patterns as shown in figure 5. The test sequence for each pattern was as follows: (1) the CV-340 was positioned so that the Aircraft Reference Point (ARP) (indicated by a block arrow painted on both sides of the aircraft) was directly over site 1 on the runway; (2) cinetheodolite tracking was begun and the airplane was taxied into position for takeoff; (3) the aircraft took off to the north and made a right climbing turn, leveling off at 458 m (1500 ft); (4) the aircraft then flew parallel to the runway until X = −12,200 m (−40,000 ft); (5) a 180° turn was then executed; (6) the final approach was flown using a 3° glide slope; (7) the airplane was landed and stopped with the ARP directly over site 1, and (8) the cinetheodolites were stopped.

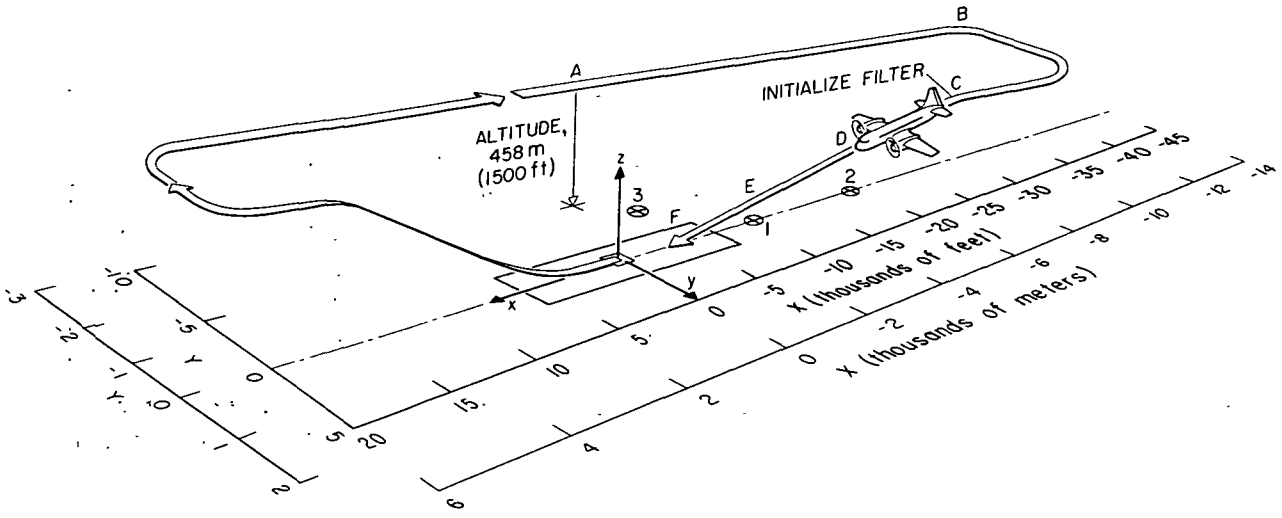

Figure 5. – "RACETRACK" flight-test pattern.

RAINPAL SOFTWARE

General Description

The RAINPAL software is an integrated software package designed to provide Kalman filter aided inertial navigation computations and communication with input/output peripherals allowing in-flight navigation with real-time data (ref. 7) or postflight navigation in a ground-based laboratory data analysis facility (see fig. 6) using recorded flight data.

The RAINPAL software incorporates three navigation operational modes: (1) a ground alignment mode, (2) a "data start" or in-flight alignment mode, and (3) the normal Kalman filter aided inertial navigation mode. These modes operate in real time or with flight data recorded in real time. The ground alignment mode serves to initialize the navigation equations and the Kalman filter before flight. The "data start" in-flight alignment mode serves the same purpose when initialization is done during flight and is also the mode used to process the data recorded at WSMR. In this latter case, ranges or other NAVAID measurements are used to calculate the required initial conditions. In any case, once the computations are complete in either of the first two modes, the system is then placed into the third or aided inertial navigation mode.

The software also provides a variety of input/output capabilities designed to facilitate the validation, testing, and operation of the RAINPAL system. These include strip chart and line printer outputs, typewriter input/output, and magnetic tape recording. The input/output functions time share with the navigation calculations using a system of priority interrupts.

Laboratory Operation of the RAINPAL Software

The laboratory facilities at Ames include an XDS-920 computer identical to that on the CV-340 aircraft. This allows the RAINPAL software to be operated in an identical manner either onboard the aircraft or in the laboratory. This laboratory facility was called the RAINPAL Ground-Based Data Analysis System. By virtue of the software and its input/output flexibility, this system, when used with recorded flight data, becomes a very powerful navigation system design and validation facility. This facility has proved invaluable for (a) validation of the RAINPAL airborne test equipment (fig. 3), (b) validation of the airborne real-time navigation functions, and (c) postflight analysis of the data recorded during the WSMR flight tests. When used for postflight analysis, the use of time-tagged data recorded in real time during flight allows the RAINPAL navigation calculations to be executed in a manner identical to that which could have been or were performed in real time onboard the aircraft. The navigation performance results presented in this report were obtained in the manner just described. A detailed description of the processing of the WSMR flight data is presented in the next section.

Processing of the Recorded Flight Data

Figure 6 is a diagram of the information flow in the laboratory facility when it was used for processing the WSMR flight data. Processing begins by reading a block of time-tagged data from a magnetic tape written by the airborne test equipment (fig. 3) during the flight test at WSMR. The time-tag allows an accurate correlation of the recorded data and the WSMR cinetheodolite solutions.

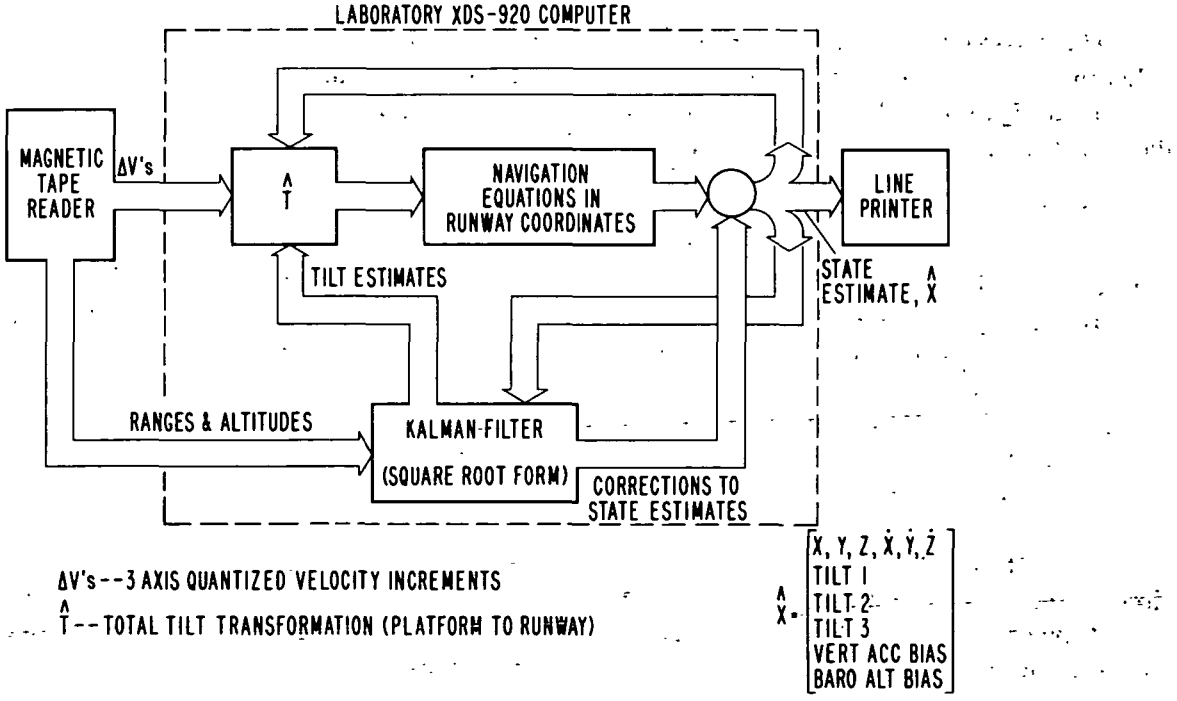

Figure 6. – Block diagram of RAINPAL ground-based data analysis system.

The inertial data are in the form of velocity changes ΔV_x, ΔV_y, and ΔV_z as 12-bit digital words from the magnetic tape. These ΔV terms result from integrating acceleration signals from the LTN-51 Inertial Measurement Unit (IMU) over a fixed time increment. The time increment is set by the rate of the precision interrupt source onboard the aircraft. These velocity changes are then transformed into runway coordinates. In the navigation equations, after the effect of the computed gravity is removed and coriolis corrections made, a second integration is performed to obtain position.

The output of the navigation equations is a six-state vector of positions and velocities of the aircraft in runway coordinates. As shown in figure 6, this state vector is used by the Kalman filter, together with the range and altitude measurements read from the magnetic tape, to compute corrections to these positions and velocities as well as estimates of five additional states. These five additional states consist of three errors (IMU platform "tilts") in the transformation $\hat{T}$ and biases in the barometric altimeter and the vertical accelerometer in the IMU. The Kalman filter state vector, $\hat{X}$, thus has eleven components that are output on a line printer for comparison with the WSMR data. The Kalman filter produces these estimated corrections from the samples of ACPRS and altimeter data read from the magnetic tape. If, for any reason, a data sample from any or all data sources is considered "bad" by a data validity test, these data samples are not processed by the filter. For the results presented in this report, data were sampled for processing by the filter at a rate of once every 2 seconds. This data rate is consistent with the real-time capability of the RAINPAL system navigating in actual flight.

Data Rejection

Precision navigation during approach and landing requires that the RAINPAL system reject bad data that might occur from a data source and cause a corrupted estimate of the aircraft state. For example, as the aircraft flies past one of the ACPRS transponders, the signal from this transponder can be either lost or become so weak that the ranges are not usable or are quite noisy. Examples of the meaningless ranges obtained from the ACPRS as a result of loss of signal are shown in figure 7.

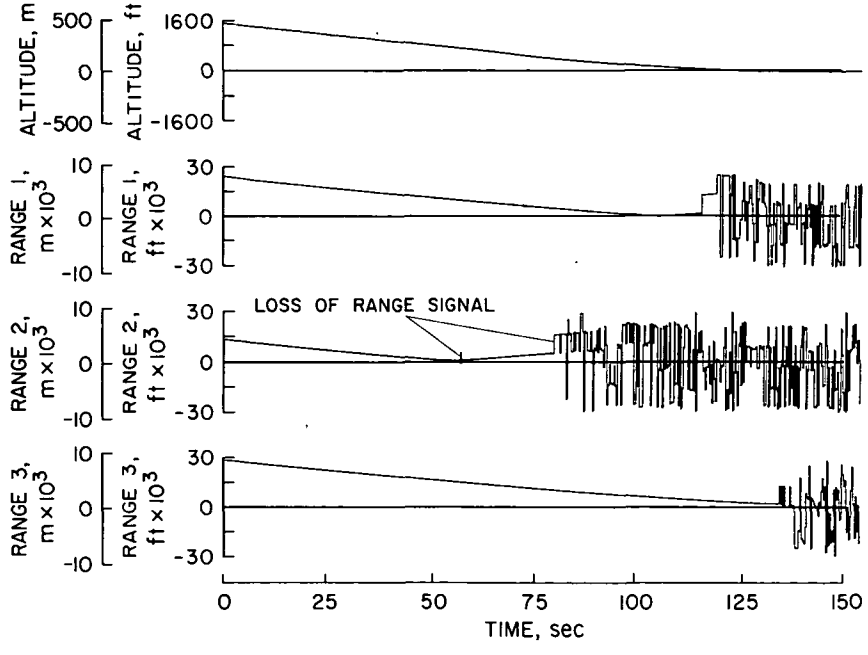

Figure 7. – Recording of ACPRS ranges and radar altimeter.

In this figure, the ranges are generally good until after the aircraft has overflown the transponder. Bad data from each data source were rejected by a validity test as follows:

(1) Each measurement residual, ΔM, is computed. (ΔM is defined as the meausrement quantity minus the estimated quantity computed from the estimated state given by the navigation system output.)

(2) The measurement is considered acceptable if

$$|\Delta M| \leqslant 2q \tag{1}$$

where q is the computed standard deviation of the measurement residual, ΔM. The minimum value of q is the standard deviation of the error in the particular measurement source and is given under Error Models.

Kalman Filter Initialization

Large initial position and velocity errors can cause a convergence difficulty in the Kalman filter. To circumvent this problem in an actual system, the program must have a built-in "data-start" procedure (in-flight alignment mode) that computes reasonably accurate initial position and velocity estimates from data (external measurements) before processing data with the Kalman filter.

For these tests, the data-start procedure directly computes the position and velocity components based on measured ranges from ACPRS transponders 1 and 3 (see fig. 1) and the barometric altimeter. The data start consists of a "least-squares" fit of straight lines through five successive samples of each measurement. The measurement averages at the center are projected ahead of real time using the straight-line average from the least-squares fit. The starting position (X, Y, Z) and the starting velocity ($\dot{X}$, $\dot{Y}$, $\dot{Z}$) are then directly calculated using a "trilateral-type" computation. Typical results of this computation at two time points referenced to the time the Kalman filter initialization began (t = 0) for the third landing are given in terms of deviations from the WSMR computed values.

As shown in table 2, the data-start procedure provides quite accurate initial condition estimates, although there are biases in these estimates. These biases are due to the fact that the estimates were obtained from range measurements that were not compensated for systematic ACPRS errors (see later discussion).

Large initial condition errors can, in some instances, cause Kalman filter estimates to diverge from the correct values because the Kalman filter algorithm assumes that the measurements are linear functions of the aircraft state when, in fact, they are not. Techniques have been developed to overcome this problem but were not included in the RAINPAL software because, with initial errors of the magnitude shown in table 2, quite rapid convergence to very small estimation errors was achieved by the RAINPAL Kalman filter algorithm. This implies that the assumption of linearity is valid for initial errors of the magnitude shown in table 2. No attempt was made to determine the range of data-start errors which the Kalman filter algorithm can handle without special provisions to account for measurement nonlinearities.

TABLE 2. – TYPICAL DEVIATIONS IN THE DATA-START COMPUTATIONS

State Component	Deviations from WSMR at t = 6.5 sec	Deviations from WSMR at t = 21.3 sec
X	-10.2 m (-33.5 ft)	-9.2 m (30.1 ft)
Y	6.7 m (22.1 ft)	6.3 m (20.6 ft)
Z	3.1 m (10.1 ft)	6.2 m (20.4 ft)
$\dot{X}$	-0.21 m/sec (-0.70 ft/sec)	0.28 m/sec (0.91 ft/sec)
$\dot{Y}$	-2.92 m/sec (-9.56 ft/sec)	-1.60 m/sec (-5.25 ft/sec)
$\dot{Z}$	-1.10 m/sec (-3.61 ft/sec)	-1.19 m/sec (-3.89 ft/sec)

Error Models

Introduction – This section describes the mathematical models that characterize the measured quantities processed by the Kalman filter. These models describe two types of errors – random and systematic. The Kalman filter requires a statistical model of the random errors and assumes that all systematic errors have been removed or are estimated as separate filter states as is done with the barometric altimeter bias. Failure of the errors in the measurement quantities to agree with the Kalman filter statistical model can have a very deleterious effect on the Kalman filter estimation performance, particularly when these modeling errors are systematic errors. The removal of such an unexpected systematic error in the ACPRS range measurements through the use of a model of the error generation process will be described. A statistical model in terms of a bias and standard deviation is given for each measurement source.

Altimeters – Two altimeters were used during the approach and landing. The barometric altimeter was used until the aircraft had descended below 22.9 m (75 ft), at which time a switch was made to the radar altimeter. The switch in altimeters was required for two reasons: (1) the radar altimeter is not independent of the terrain over which the aircraft is flying and can only be relied upon shortly before touchdown when the aircraft is over flat terrain in front of the runway, and (2) the barometric altimeter bias changed rapidly due to large dynamic errors in the pitot-static system induced by the pitchup of the aircraft at landing. This could result in large Z axis errors, which, at touchdown, have been observed to be on the order of 21.4 m (70 ft).

Each altimeter signal was fed through two isolation amplifiers with different gains into separate analog-to-digital (A/D) converter channels to provide a "high" and a "low" scale. The scales were:

(a) Barometric altimeter: 0-305 and 0-3050 m (0-1,000 and 0-10,000 ft)

(b) Radar altimeter: 0-381 and 0-1525m (0-1,250 and 0-5,000 ft)

The altitude of the Northrup Strip was approximately 1220 m (4000 ft). This considerably exceeded the range of the barometric altimeter low 0-305 m scale. To make this channel usable, an offset electrical bias equivalent to 1207.3 m (3958.5 ft) was introduced into the isolation amplifier for the low scale.

Two altimeter scales were used to minimize the effect of A/D-induced noise. Unfortunately, apparent grounding anomalies in the isolation amplifiers introduced an additional source of noise into the altimeter signals. The amplitude of this noise varied from day to day. For the flight tests reported here, the standard deviation was about 2 m on the low scale and about 10 m on the high scale. Careful redesign of the amplifiers probably could reduce the standard deviation of this noise by a factor of 4 or 5.

The standard deviation of the errors in the recorded barometric altimeter data used in the post-flight analysis was 4.58 m (15 ft) for both the high and low scales. A bias value of −27.45 m (−90 ft) was determined on the ground just before the test as nominal compensation for the local atmospheric pressure. This same bias was used for each of the three landings.

The radar altimeter error model used in the Kalman filter was for noise only. A bias was used to compensate the data for an observed offset introduced primarily by the isolation amplifier. The standard deviation used in the filter and the bias (offset compensation) were as follows: Standard deviation, 1.83 m (6.0 ft); and bias, 5.19 m (17 ft).

ACPRS – Early attempts to use the RAINPAL ground-based data analysis facility for postflight processing of the data recorded at WSMR indicated an anomalous behavior of the ACPRS ranges that appeared to become worse as the aircraft approached touchdown. Examination of the difference between the measured ACPRS ranges and the WSMR computed ranges indicated a behavior pattern as shown in figure 8. In this figure, ACPRS range errors are shown as dots for each of the three

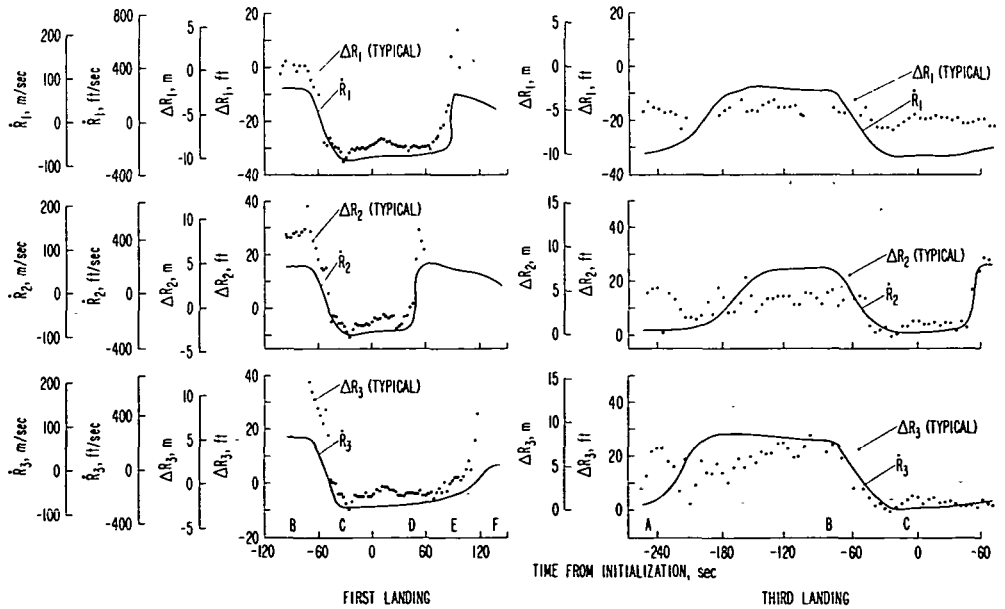

Figure 8. – Range errors and range rate to each transponder.

ranges. On the left side of the figures are the range errors for the first landing and, on the right, the range errors for the third landing. Also shown in this figure are plots of the respective range rates. The range-rate plots are shown to a scale that accentuates the correlation of the range errors and range rate. The curves for the first landing start at point B (see fig. 5). The curves for the third landing start earlier, beginning at point A and terminating about 70 seconds before touchdown. The curves starting at point A show the range-rate effect in that portion of the flight when the aircraft was facing the backside of the transponder antennas.

From this figure, it appears that there is a striking dependence of range error on range rate. In addition, it also shows the following:

(a) There is an apparent dependence on signal strength. When the aircraft is farther away from the transponder or the aircraft antenna is not pointed directly at the front side of the transponder antennas, the range errors tend to be reduced.

(b) There is an apparent time dependence. Comparison of the errors on first landing with those on the third landing indicate that the errors reduce with time.

Examination of these data, of data from flights at WSMR on other days, and of functional block diagrams (ref. 9) and discussions with the manufacturer of the ACPRS system has led to two inherent circuit deficiencies that appear to be responsible for the Doppler-like error. Relatively simple changes in circuit design or gain adjustments could possibly overcome these deficiencies.

To evaluate the navigation performance that could be attained with the "improved" ACPRS, a mathematical model of the range error generation process was required which could be implemented with software. Such an improvement is one means of overcoming hardware deficiencies and giving an improved ACPRS. Examination of the ΔR and $\dot{R}$ histories in figure 8 indicates that a good model would be of the form

$$\Delta R_i = B_i(v) + K_i(v)\dot{R}_i \tag{2}$$

where i denotes the transponder number and $B_i(v)$ and $K_i(v)$ are nonlinear functions of the AGC voltage, v, for channel i. The range rate, $\dot{R}_i$, is computed from the current best estimate of the state at the particular point along the flight path. The AGC voltages were not recorded during the WSMR tests. As a result, a compensation of the form of equation (2) with nonlinear coefficients could not be tested. Instead, data were processed during approach and landing where the major portion of the error in each of the three ACPRS ranges was a linear expression of the form:

$$\Delta R_{ci} = B_i + K_i\dot{R}_i \; ; \quad i = 1, 2, 3 \tag{3}$$

Equation (3) was used from point C to touchdown since this portion of the flight was of primary interest. The $\dot{R}_i$ terms were computed along the flight path each time ACPRS range measurements were to be processed using the expression

$$\dot{R}_i = \frac{1}{R_i}[\dot{X}(X - X_{oi}) + \dot{Y}(Y - Y_{oi}) + \dot{Z}(Z - Z_{oi})] \; ; \quad i = 1, 2, 3 \tag{4}$$

where

$$R_i = [(X - X_{oi})^2 + (Y - Y_{oi})^2 + (Z - Z_{oi})^2]^{1/2} \quad ; \quad i = 1, 2, 3 \tag{5}$$

The terms X_{oi}, Y_{oi}, and Z_{oi} are the antenna coordinates of the three transponders given in table 1 and the state elements X, Y, Z, $\dot{X}$, $\dot{Y}$, and $\dot{Z}$ are the estimated values referred to the ACPRS antenna in the nose of the CV-340.

Figure 9 shows a comparison of the actual range errors (dots) and the range error calibration computed from equation (3). The curves on the left were computed during the first landing and those on the right during the third landing. The constant coefficients used in equation (3) for each transponder are given in table 3 where range rate is measured in meters per second and ΔR_c is in meters.

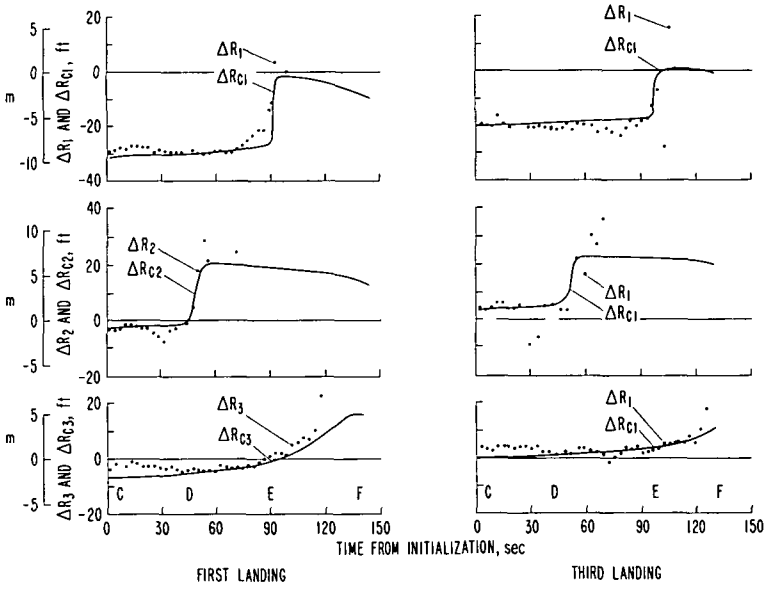

Figure 9. – Comparison of range errors and model of range errors.

TABLE 3. – COEFFICIENTS FOR IN-FLIGHT COMPUTATION OF ΔR_c

Transponder	First landing		Second landing		Third landing	
i	B_i	K_i	B_i	K_i	B_i	K_i
1	-4.33	0.06170	-2.74	0.0530	-2.50	0.0446
2	3.05	.04547	4.02	.0471	4.42	.0429
3	4.11	.07500	3.07	.0345	3.60	.0429

As stated earlier, the ACPRS range errors diminished in amplitude with time (ref. 9). As a result, the calibration model (eq. (3)) tended to be less in error during the later landings, which caused a trend toward improved navigation accuracy as the flight tests progressed. The effect of imperfect modeling and therefore calibration for the range rate induced errors is to produce navigation performance which is slightly pessimistic when compared to the performance that would be expected from flight tests using a hardware improved ACPRS.

After the range error calibration (eq. (3)) was applied, the statistical model of the random ACPRS range errors used in the Kalman filter was: standard deviation, 0.91 m (3.0 ft); and bias, 0.0 m.

FLIGHT-TEST RESULTS

Flight-Test Operations

The flight-test operations were controlled from the WSMR King 1 control station via UHF radio to the pilot of the test aircraft. Aircraft position as measured by an FPS-16 radar was fed to a plot board at the control station for comparison with a trace of the desired flight pattern. During the test, the WSMR Vector Controller would compare the actual path of the aircraft to the desired path and radio the necessary course changes to the pilot. Also at the plot board were (1) the WSMR Radar and Cinetheodolite Controllers and (2) four members of the NASA test team whose function was to provide program direction, monitor all UHF radio transmissions, advise the CV-340 pilots via radio, and keep accurate logs of all events during the test.

Reduction of WSMR Cinetheodolite Data

Description of the cinetheodolite system – A cinetheodolite is a precision device for measuring azimuth and elevation angles. At WSMR, 35-mm motion pictures are taken of the object being manually tracked by an operator who observes the object through a telescope. The azimuth and elevation angles of the theodolite gimbals (center of photograph) are recorded on each frame of the film along with the time. Cinetheodolites are operated in networks since, without range information, position cannot be determined from a single cinetheodolite. With proper placement of the cinetheodolites in a network, the three position components of the tracked object can be determined to approximately equal accuracy. All cinetheodolite photography is synchronized electrically through an underground cable. In this instance, photographs were taken once every second. The number of cinetheodolites in a network being used for data reduction at any particular time may vary, depending on the position of the object being tracked or on other factors such as the number of photographs available in the film load. Seven cinetheodolites were assigned to the tests described in this report.

When the film from a flight test is developed, it is manually examined frame by frame and corrections to the gimbal angle readings determined so that, in this case, the angle readings correspond to the Aircraft Reference Point (ARP), that is, the tip of a black arrow painted on each side of the aircraft.

Computation of position and velocity – WSMR uses an extensive digital computer program to take the gimbal angles at each time point (along with the coordinates of each cinetheodolite station) and compute a set of position components ($\bar{X}$, $\bar{Y}$, $\bar{Z}$) that "best" fits the angle data. A conventional least-squares procedure is then used (ref. 10) to fit a second-order curve of the form

$$X(t_j) = A_0 + A_1 t_j + A_2 t_j^2 \; ; \quad j = 1, 2, \ldots, N (3 \leqslant N \leqslant 21) \tag{6}$$

through a series of N time points to find values for A_0, A_1, and A_2. Expressions similar to equation (6) are used to find equivalent A values for $Y(t_j)$ and $Z(t_j)$. The X value at any time t_n on the curve is then found by substituting t_n into equation (6), with Y and Z being found in a similar way. The resulting X, Y, and Z are the WSMR estimates of the aircraft position at t_n.

The corresponding X velocity estimate is found by differentiating equation (6) with respect to t_j. The resulting expression is

$$\dot{X}(t_j) = A_1 + 2A_2 t_j \; ; \quad j = 1, 2, \ldots, K \tag{7}$$

Similar expressions are used for $\dot{Y}(t_j)$ and $\dot{Z}(t_j)$. The velocity components are found by evaluating the curve at its midpoint using equation (7) and the equivalent $\dot{Y}$ and $\dot{Z}$ expressions. This same procedure is repeated at the next time point in the time history and so on in what is called a "moving arc" technique.

Cinetheodolite position and velocity error statistics – To estimate the RMS error (1-σ) in each of the three position components, the computed point (X, Y, Z) is used to compute the azimuth and elevation from each cinetheodolite station. The differences between the computed azimuth and elevation angles and the measured values are found and these residuals are used to calculate a sample angular variance, S_A^2. Partial derivatives derived from the least-squares solution principal matrix are then used to compute C_x so that the WSMR estimated 1-σ error in each position component may be found from an expression of the form

$$\hat{\sigma}_x = (C_x S_A^2)^{1/2} \tag{8}$$

Similar expressions are used to find $\hat{\sigma}_y$ and $\hat{\sigma}_z$.

Estimates of the RMS error in the velocity components are found by first computing a sample variance, $S_{\dot{x}}^2$, using the squares of the differences between the least squares $X(t_j)$ from equation (6) and $\bar{X}(t_j)$ from the cinetheodolite solution. This sample variance is then scaled using partial derivatives obtained from the principle matrix of the least squares solution, that is,

$$\sigma_{\dot{x}} = (C_{\dot{x}} S_{\dot{x}}^2)^{1/2} \tag{9}$$

The terms $\hat{\sigma}_{\dot{y}}$ and $\hat{\sigma}_{\dot{z}}$ are found in an analogous way.

The computed estimates of the positions and velocities along with the associated estimates of the RMS error in these estimates of the aircraft state were published by WSMR for 1-sec time intervals. These data are used in this report to evaluate the performance of the RAINPAL system.

Cinetheodolite Static Checks

Static checks of the WSMR cinetheodolite tracking system were included as part of the flight-test procedures. The purpose of these static checks was to gain insight into the accuracy and error characteristics of the trajectory estimates obtained from the cinetheodolite tracking system. Ultimately, it was expected that the insight gained would aid in understanding and interpreting the WSMR in-flight estimates. The static checks were included in the flight-test procedures in the following manner: after each landing, the aircraft was taxied to site 1 and positioned so that the aircraft reference point (ARP) was approximately over the surveyed site. Then the X, Y, and Z components of the ARP with respect to site 1 were surveyed to an accuracy of ±0.076 m (±3 in.) and recorded for later comparison with WSMR estimates derived from the cinetheodolite data.

Table 4 is a summary of the analysis of the WSMR estimates during the time periods the aircraft was stopped at site 1 after each landing using the known position and velocity (zero) as a reference. The analysis was based on 8 seconds (8 data points) of data for the first landing (the cinetheodolites were stopped too soon) and on 40 seconds of data for the second and third landings. The first column for each landing in table 4 shows the mean (average) error in the WSMR estimates for each of the three components of position and velocity. The second column shows the standard deviations of these errors. The third column shows the mean of the standard deviations (1 σ) quoted by WSMR as representing the uncertainty in the cinetheodolite-derived estimates (see eqs. (8) and (9)).

TABLE 4. – WSMR STATIC CINETHEODOLITE TRACKING ERRORS

Components	First landing			Second landing			Third landing		
	WSMR mean tracking error	Observed 1-σ values	Mean quoted 1-σ values	WSMR mean tracking error	Observed 1-σ values	Mean quoted 1-σ values	WSMR mean tracking error	Observed 1-σ values	Mean quoted 1-σ values
X (m)	-1.74	0.15	1.95	0.00	0.08	0.55	0.11	0.11	0.58
Y (m)	.73	.36	1.86	.21	.44	1.10	.04	.41	1.19
Z (m)	-1.58	.19	1.16	-.12	.08	.47	-.30	.11	.49
$\dot{X}$ (m/sec)	.155	.155	.034	.006	.098	.015	.003	.094	.015
$\dot{Y}$ (m/sec)	-.064	.719	.100	-.061	.314	.049	.015	.500	.076
$\dot{Z}$ (m/sec)	-.018	.235	.034	.000	.061	.009	-.012	.128	.021

The data in table 4 provide considerable insight into cinetheodolite tracking system performance. Comparisons of the mean tracking error for the three landings show a bias level in the X and Z position components of almost 1.8 m (6 ft) for the first landing. These levels for the second and third landings were generally less than 0.3 m (1 ft). WSMR has stated that this difference was caused by an additional cinetheodolite being used in only the first landing solution as the aircraft approached the ground and that this cinetheodolite has a bias error whose effect could not be removed. Aside from this discrepancy on the first landing, column 1 for each landing shows that the mean value is an accurate estimate of the true position and velocity when the aircraft is stationary.

The statistical data in columns 2 and 3 show substantial discrepancies between the observed sample standard deviations (column 2) and the 1-σ values quoted by WSMR as representing the accuracy of the WSMR estimates. Furthermore, there is a lack of self-consistency in the quoted 1-σ values. The quoted 1-σ values given for position estimates (column 3) appear to be pessimistic (by a factor of 2 to 5) when compared to the observed sample standard deviation in column 2. In velocity, the opposite is true – the quoted 1-σ values are optimistic (by a factor of 5 to 7). Another type of inconsistency (not shown in table 4) is apparent when WSMR-quoted 1-σ values for the static tests are compared with those for periods when the aircraft was in flight. Intuitively, it would seem that random tracking errors should be significantly smaller when the aircraft is stationary. The static velocity 1-σ values quoted for $\dot{X}$ and $\dot{Z}$ (column 3) are about an order of magnitude smaller than the in-flight values. However, the quoted X, Y, Z, and $\dot{Y}$ 1-σ values are about the same regardless of whether the aircraft is flying or stationary on the ground.

Plots were made of the observed data from which the standard deviations in column 2 were derived. The plots (not shown) showed frequent large fluctuations approximately evenly distributed about the mean value. For the third landing, the maximum and minimum values for these fluctuations were:

± 0.27 m (± 0.9 ft) in X

± 0.95 m (± 3.1 ft) in Y

± 0.30 m (± 1.0 ft) in Z

± 0.24 m/sec (± 0.8 ft/sec) in $\dot{X}$

± 0.95 m/sec (± 3.1 ft/sec) in $\dot{Y}$

± 0.30 m/sec (± 1.0 ft/sec) in $\dot{Z}$

Comparisons of these plots with the in-flight data plots show rather good agreement between the character and magnitude of the fluctuations observed in the flight data (fig. 10) and those observed on the ground. This tends to indicate that the in-flight fluctuations are due not to aircraft motion but to the same source as the fluctuations observed on the ground.

The reason for the differences between the observed 1-σ values and the quoted 1-σ values is probably associated with unrealistic error models implicit in the equations used to compute the quoted 1-σ values. For example, when the aircraft is stationary on the ground, the constants A_1 and A_2 in equation (6) should have been zero but they were not. Because of these differences, the

quoted 1-σ values are of limited use for assessing RAINPAL performance. However, the following conclusions appear reasonable: (1) Although the quoted static 1-σ values for WSMR position estimates are too large, the quoted values for in-flight situations are nearly correct; (2) the quoted velocity 1-σ values should be increased by a factor of about 6 or 7 for both the static and in-flight situations since this makes them consistent with the observed sample statistics in the static checks and consistent with the random fluctuations observed in the WSMR velocity estimates in the in-flight situations; and (3) the mid-value of the upper and lower bounds of the random fluctuations is usually a good estimate of the correct position or velocity for the static situation. The similarity of the fluctuations seen in both the static and in-flight situations implies that this same conclusion may also apply in flight for velocity data and, in most cases, for position data.

Navigation Performance

Postflight analysis procedures – The RAINPAL software was used in the ground-based laboratory data analysis facility to obtain estimated flight trajectories. The navigation performance was then determined by comparing these RAINPAL estimated flight trajectories with the trajectories measured by the WSMR cinetheodolite tracking system. This comparison was made using data recorded in flight during three separate landings on the same day.

Data were recorded at WSMR at a rate of four times per second. However, the Kalman filter processed data once every 2 seconds. As a result, only 1/8 of the recorded measurement data could be processed in determining a particular RAINPAL estimated flight trajectory. Depending on the filter initialization time, eight different estimates of the same trajectory can be obtained by sequentially shifting the starting time of each estimate of the trajectory by increments of 1/4 second. Therefore, each of the eight possible estimated trajectories uses different samples of the measurement data. Each trajectory uses the same inertial data so that the resulting dispersions in the estimated aircraft state resemble those that would be obtained if the aircraft were flown over the identical path eight times. Only three of the eight possible estimates are shown in this report to enhance the clarity and readability of the figures.

During the flight test, a slow drift in the accelerometer biases was detected but the cause was not located and removed until after the flight tests. To obtain the results presented here, a refinement was made in each of the three accelerometer biases using a postflight calibration procedure.

Comparison of RAINPAL and WSMR estimated trajectories – Comparisons of RAINPAL and WSMR estimated trajectories are presented in figure 10. Most of these data are presented for the final 40 seconds of flight before touchdown for three different landings. This is because RAINPAL is intended to provide the most accurate estimation performance in the final portion of each landing. This choice provides for figures with scales whose resolution is consistent with this objective of the RAINPAL system. The X position component (along track) will not be shown because the X distance covered in the final 40 seconds would result in a scale in which the difference between the WSMR and RAINPAL results would be indistinguishable. However, a comparison of the RAINPAL and WSMR data was made at the vicinity of touchdown. From this comparison, it is estimated that the standard deviation of the error in the RAINPAL X-position estimates is in the range 0.9 ±0.6 m (3 ±2 ft). Figures 10(a) and 10(b) compare three RAINPAL estimated trajectories with the WSMR estimated trajectory. The WSMR results are presented in terms of plus and minus 1-σ bounds about

their estimate of the aircraft trajectory. These 1-σ bounds are the standard deviations quoted by WSMR for the error in their estimates.

Figure 10(a) presents the Y component. The WSMR cinetheodolite solutions show that RAINPAL system navigation performance in the Y component improved in going from the first to the third landing. This is consistent with the data and discussion in connection with figure 9, where the ACPRS range error calibration errors were smaller for the third landing. The results obtained for the third landing are more indicative of the navigation performance that could be expected for a precision ranging system which did not have the range-rate error anomaly observed in the ACPRS system. This figure shows (when going from the first to the third landing) the effect on navigation performance of errors in the ACPRS calibration. In this case, the ACPRS calibration errors caused the Y error at first landing touchdown to range from about 2.4 to 4.3 m (8 to 14 ft), but for the third landing, where these errors were much smaller, the touchdown dispersion range was only about 0.9 to 1.8 m (3 to 6 ft). On the basis that the third landing is more indicative of the actual capability of the RAINPAL system, the standard deviation of the Y-position error at touchdown is estimated to be in the range 1.2 ±0.6 m (4 ±2 ft).

Figure 10(b) compares the Z component of the three RAINPAL estimates to the WSMR determined Z position for each of three landings. This figure shows very good agreement between the WSMR and RAINPAL estimates until the aircraft reaches an altitude of about 4.6 to 6.1 m (15 to 20 ft). At this point, there is a clear divergence between the WSMR and RAINPAL estimates, with the two sets of data showing a difference of about 1.2 to 2.1 m (4 to 7 ft) at touchdown. The correct Z position at touchdown is shown on each plot. This is the Z position of the LTN-51 INS located in the baggage compartment (2.2 m or 7.2 ft above the runway) and its Z position is known when the wheels are on the ground. Examination of the plots shows that the RAINPAL system estimates were generally within 0.3 m (1 ft) of the correct value although, in one case, on the third landing the error was about 1.2 m (4 ft) high. These estimates were judged to have errors whose standard deviation is in the range 0.9 ±0.6 m (3±2 ft).

All of the WSMR Z estimates were low at touchdown, ranging in error from about 0.9 to 1.8 m (3 to 6 ft). Note that the touchdown bias remained in the WSMR data for the first landing after the aircraft had taxied the remaining 910 m (3000 ft) or so to site 1, but not for the second or third landings (as was shown in table 4). An explanation for the behavior was offered by WSMR and was discussed in connection with table 4, but it appears to the authors that this error could also be influenced by atmospheric refraction error in the cinetheodolite data. This type of error might correlate better with the increasing divergence in the data as the aircraft approached the ground and is supported, to some extent, by the fact that WSMR corrects for atmospheric refraction based only on a "standard day."

Figure 10(c) is a plot of $\dot{X}$ versus time for each of the three landings. The consistency of the RAINPAL estimates is extremely good. The agreement between WSMR and the RAINPAL estimates is generally well within 0.15 m/sec (0.5 ft/sec), which is approximately the standard deviation of this component indicated by column 2 for each landing in table 4. The WSMR data exhibit a fluctuating behavior that is probably not a result of aircraft motion since the aircrew reported no turbulence during the test and surface winds were steady at about 2 knots. Furthermore, in the discussion in conjunction with table 4, it was pointed out that the in-flight velocity fluctuations have a character similar to that observed when the aircraft was stationary on the ground and that the fluctuations are probably due to limitations in the least-squares estimation technique. It was also pointed out in the

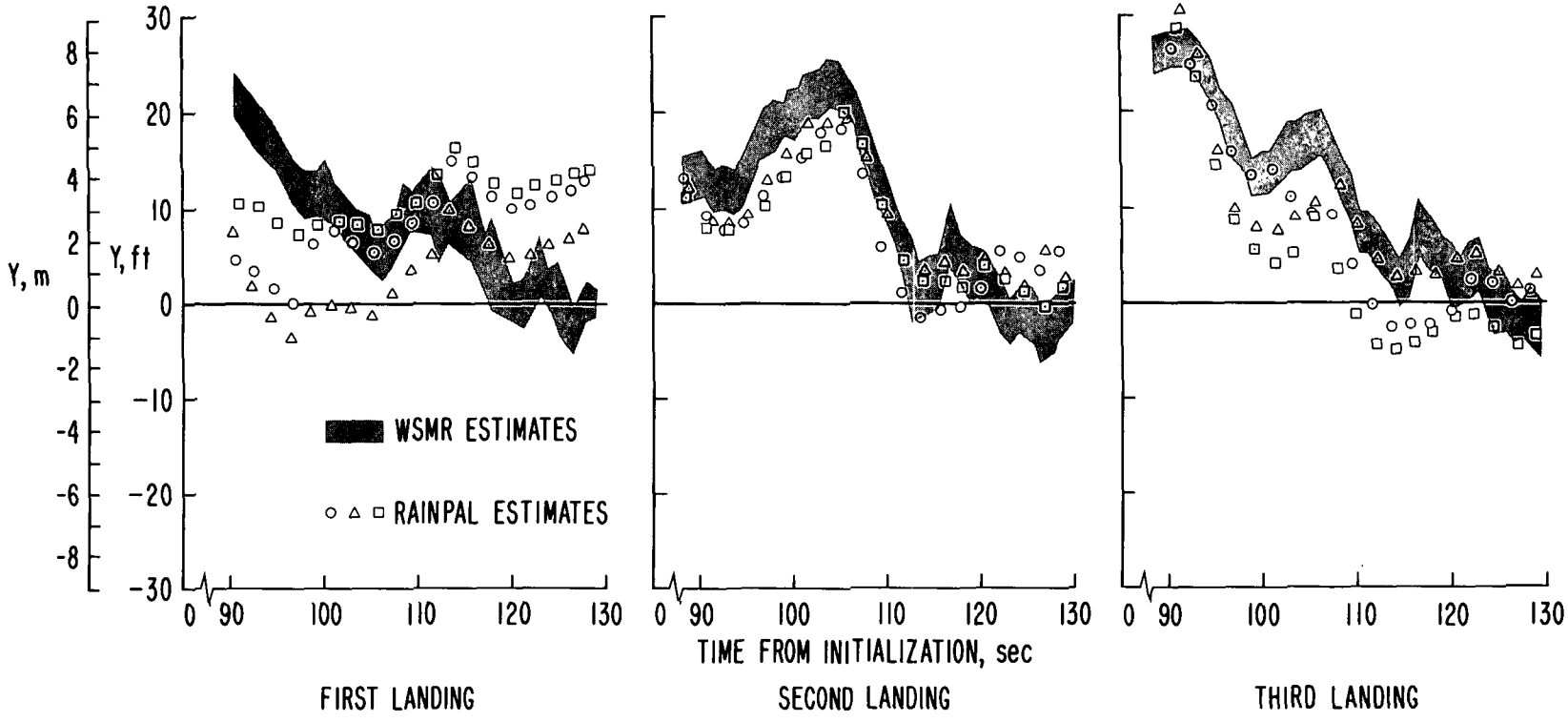

(a) $\dot{Y}$ position estimates.

Figure 10.– Comparison of RAINPAL and WSMR position estimates.

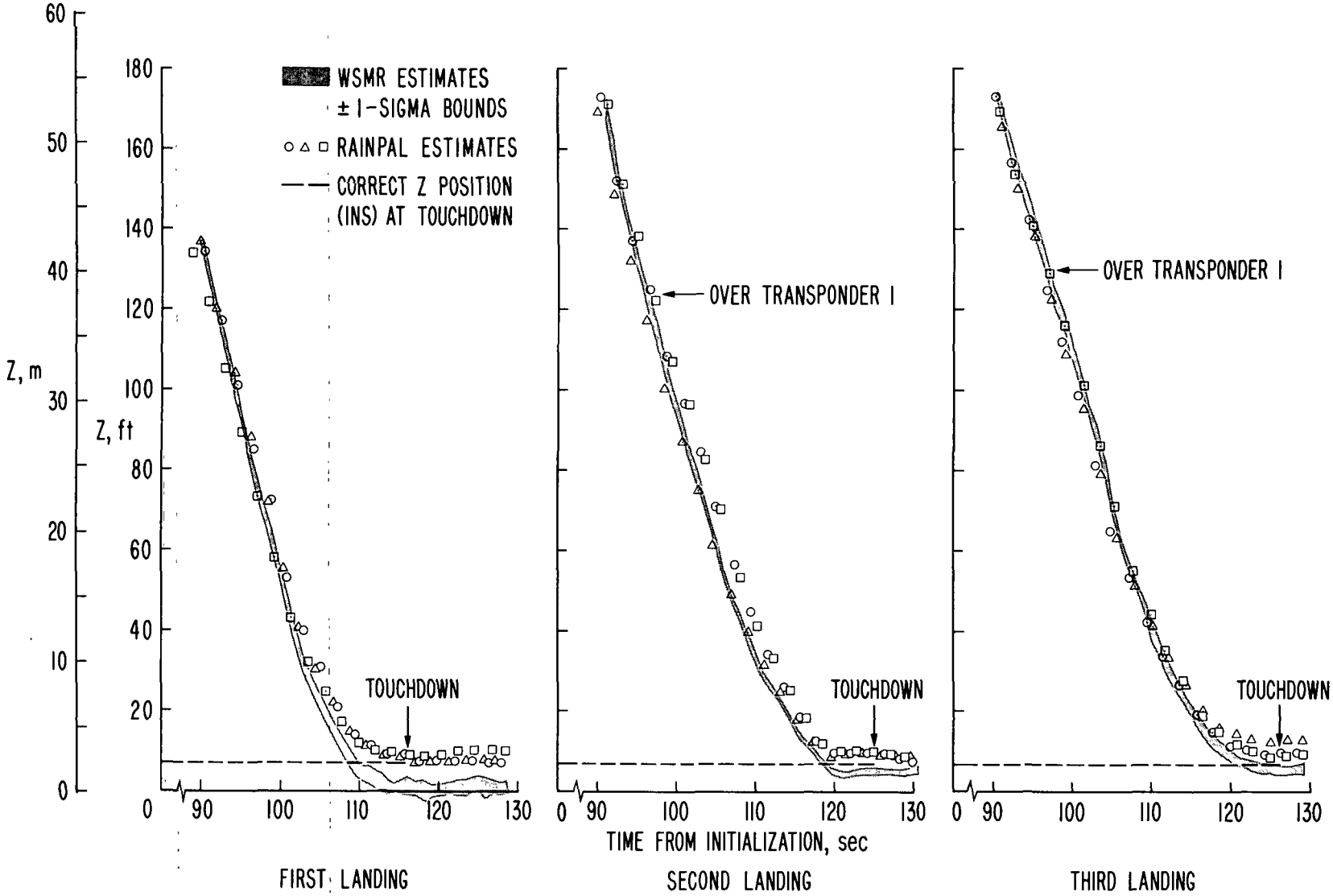

(b) $\dot{Z}$ position estimates.

Figure 10.– Continued.

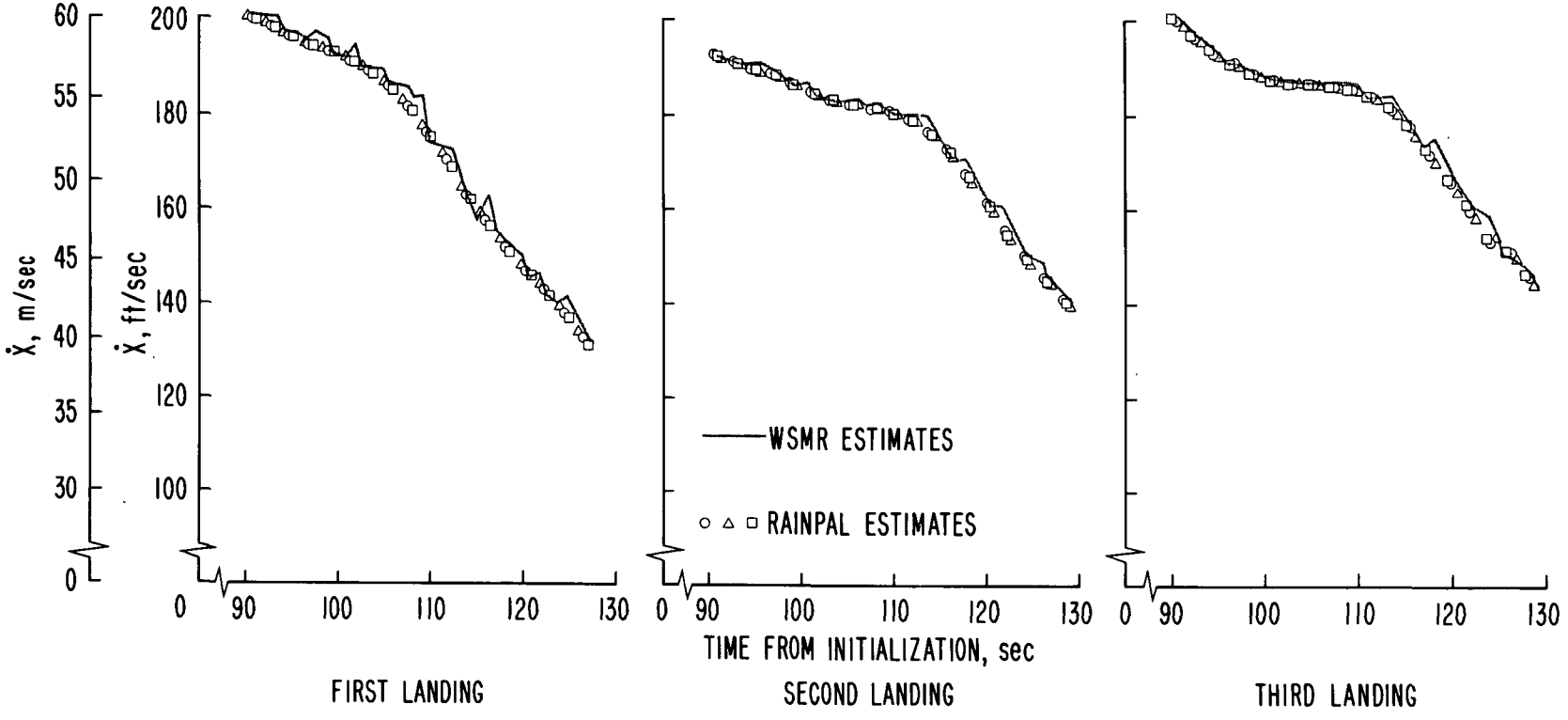

(c) $\dot{X}$ velocity estimate.

Figure 10.– Continued.

same discussion that the quoted ±1-σ values for in-flight situations were too small by a factor of 6 or 7. Hence, no ±1-σ bounds are shown for any of the WSMR velocity data in this report. Based on the data shown in figure 10(c) and the observed results presented in table 4, it is estimated that the standard deviation of the error in the RAINPAL estimates of $\dot{X}$ is in the range 0.15 ±0.06 m/sec (0.5 ±0.2 ft/sec).

Figure 10(d) is a plot of $\dot{Y}$ and $\dot{Z}$ versus time for the three landings. Again, the three RAINPAL estimates are consistent. Based on the observed results shown in table 4, variations with a standard deviation of 0.72 m/sec (2.4 ft/sec) should characterize the WSMR $\dot{Y}$ estimates on the first landing, decreasing substantially on the second and third landings. For $\dot{Z}$, table 4 indicates that reasonable values for the standard deviations of the WSMR data are on the order of 0.15 m/sec (0.5 ft/sec) for the first, second, and third landings. It is difficult to assess the probable RAINPAL $\dot{Y}$ error at touchdown because of the rather large random errors that appear to exist in the WSMR $\dot{Y}$ estimates. However, the three RAINPAL trajectories have a small dispersion in $\dot{Y}$, which is well within the ±0.46 m/sec (±1.5 ft/sec) 1-σ bounds that appear reasonable for errors in the WSMR data (see discussion in association with table 4). The RAINPAL $\dot{Y}$ error at touchdown (1 σ) is certainly not greater than about ±0.46 m/sec (1.5 ft/sec) and may be as small as 0.15 m/sec (0.5 ft/sec). For $\dot{Z}$, the results from the static tests indicate that random tracking errors (1 σ) ranging from 0.24 to 0.06 m/sec (0.77 to 0.20 ft/sec) should be expected at touchdown. The random dispersions in the RAINPAL estimates are on the order of about ±0.15 m/sec (±0.5 ft/sec). It appears reasonable, therefore to assign a standard deviation ranging from 0.15 ±0.06 m/sec (0.5 ±0.2 ft/sec) to the RAINPAL $\dot{Z}$ error.

Effects of estimating barometric altimeter bias – The barometric altimeter bias is considered to be the mean value of the much more rapidly varying altitude measurement errors. This quantity is a function of the local atmospheric pressure that is slowly changing. It is also affected by the non-constant errors in the aircraft pitot-static system. As a result, the term "barometric altimeter bias" applies not to a true bias (constant) but, considering the length of the flight test, to a relatively slowly varying quantity. It was therefore included as one of the state variables of the Kalman filter so that it could be estimated in flight when a good independent source of vertical information was available. This would occur, for example, when flying over a precision ranging system transponder (refs. 1 and 2). In contrast, the radar altimeter bias can be regarded as a true constant (bias) that can be calibrated before flight so there is no need to include it as a state variable.

To demonstrate the impact of estimating the barometric altimeter bias on the Kalman filter estimation of the Z component, one run was repeated with the barometric altimeter bias estimation feature disabled. Figure 11 shows the result of this run compared to its counterpart repeated from figure 10(b) (landing 3). This figure shows that the Z estimation without barometric altimeter bias estimation is much more poorly behaved than the comparison run. In particular, a discontinuity in Z of 12.2 m (40 ft) occurred as the aircraft passed over transponder 1 at 97 sec (dashed line). This was due to the Kalman filter receiving good vertical data for a short time while the aircraft passed over transponder 1. Later, a second discontinuity of 11 m (36 ft) occurred when the switch was made to the radar altimeter (dotted line). The figure shows that the Z estimation with bias estimation is in very good agreement with the WSMR estimates and is a smooth continuous curve without discontinuities even when the switch to the radar altimeter was made. Such discontinuities are considered important in automatic landing systems because they could result in control transients at low altitudes from which it would be difficult for the aircraft to recover before touchdown.

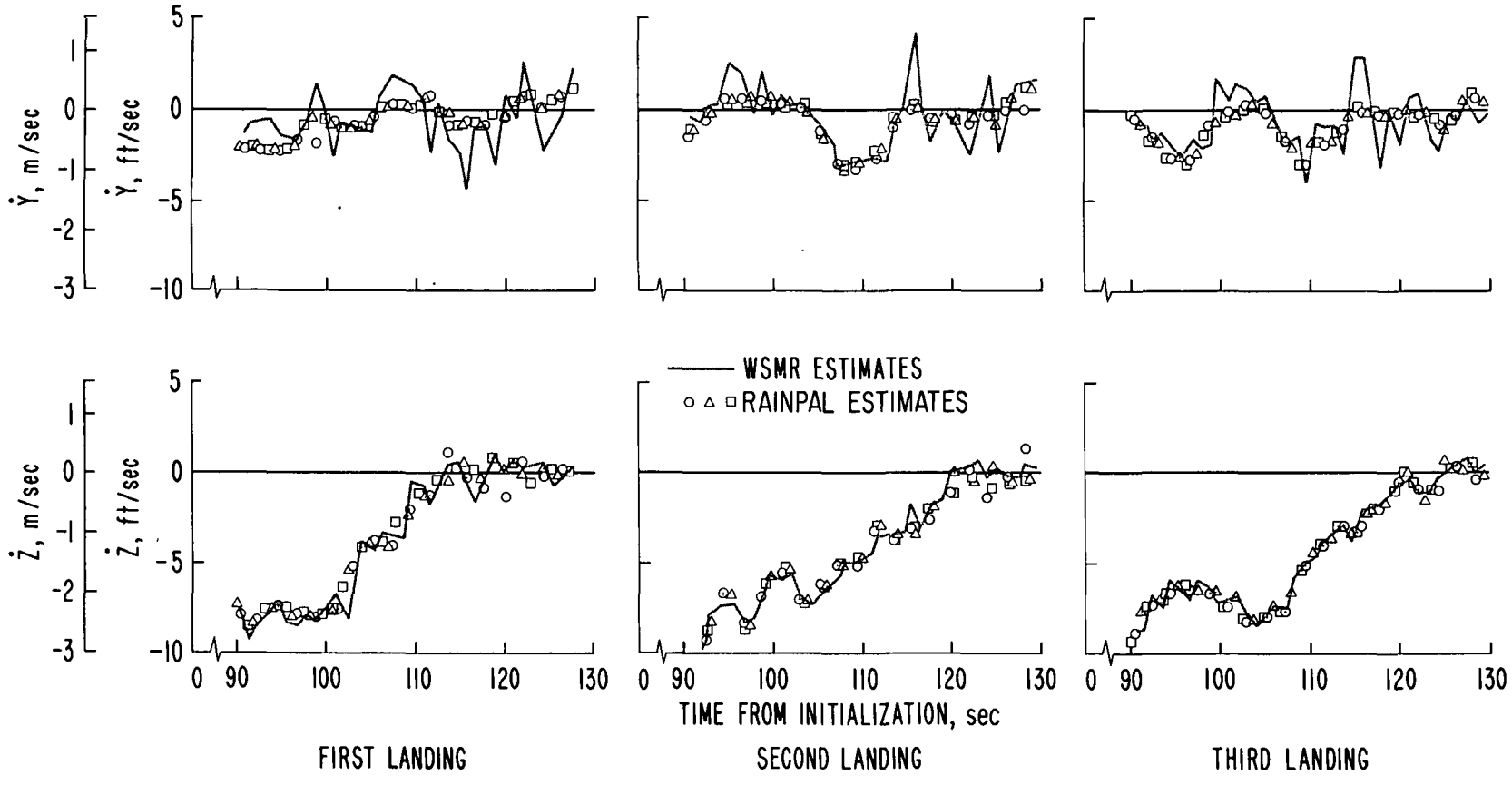

(d) $\dot{Y}$ and $\dot{Z}$ velocity estimates.

Figure 10.– Concluded.

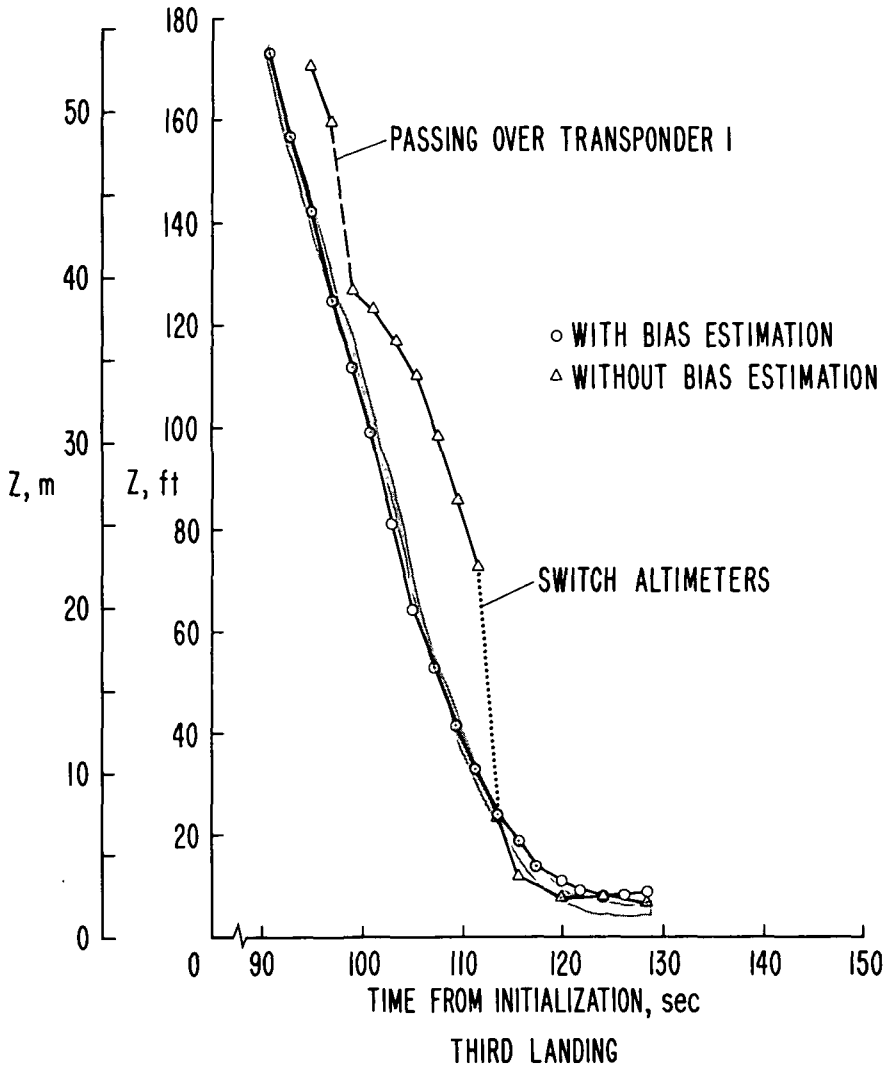

Figure 11.– Vertical channel performance with or without barometric altimeter bias estimation.

Comparison of free inertial and RAINPAL solutions – The purpose of figure 12 is threefold: (1) to show the system performance in the free inertial mode, (2) to show the improvement over free inertial navigation achieved when ACPRS and altimeter data are processed every 2 seconds, and (3) to supplement the data in figures 10 by including data before 90 seconds. Free inertial, in this case, means starting with the WSMR estimates of initial position and velocity and integrating the ΔV_x, ΔV_y, and ΔV_z data recorded on magnetic tape during the flight test at WSMR; no ACPRS or altimeter data were processed in this mode. The free inertial performance indicates the quality of key elements of the experimental inertial system operating in a runway coordinate system: These include:

(1) the quality of accelerometer, gyros, and other platform components of the LTN-51 IMU,

(2) the quality of the integration of the acceleration signals by the EIU,

(3) the correctness of the runway referenced inertial navigation equations programmed in the XDS-920 computer, and

(4) the adequacy of the fixed-point scaling used in the XDS-920 computer.

In figure 12, the WSMR estimates are used as a reference, that is, the WSMR estimates were subtracted from both the free inertial and RAINPAL estimates to give the difference quantities plotted. This procedure yields tractable plotting scales for comparing the free inertial and RAINPAL data but suffers from the fact that WSMR tracking errors appear as errors in both the free inertial and RAINPAL position and velocity estimates. Figure 12(a) shows the deviations in position obtained for the second landing.

The deviations in position and velocity shown for the free inertial operation are zero at $t = 0$ because the WSMR estimates were used to initialize the experimental inertial navigation system. On the other hand, the RAINPAL navigation system, which includes the experimental inertial navigation system, began a data-start procedure at $t = 0$, but there was no output until 16 seconds, when the procedure was completed.

Figure 12(a) shows that the deviations in free inertial position exhibit an error time history common to most unaided inertial systems. Specifically, the effect of acceleration errors first become readily apparent at about 30 seconds in the ΔY and ΔZ components and at about 50 seconds in the ΔX component. These acceleration errors, though quite small, clearly show the effect on position error of multiplying by the square of the elapsed time; after 130 seconds, this effect is significant. Even so, the errors are within the 1-n. mi./hr specification for a commercial INS such as the LTN-51.

In comparison, the RAINPAL run, in which the experimental navigation system is aided by external data, maintained the X component generally within 1.5 m (5 ft) of the WSMR estimate throughout the entire 130-second run. The Y component deviated from the WSMR value by as much as 5.5 m (18 ft) on two occasions during the first 2/3 of the time history but, in the latter third, remained generally within about 1.5 m (5 ft) of the WSMR estimate. The Z component deviated on one occasion to a maximum of about 3.4 m (11 ft) at 105 seconds (see fig. 10(b)) but (except for initial condition errors) was generally within 1 m (3.3 ft) of the WSMR estimate for a majority of the first 90 seconds.

Figure 12(b) shows the corresponding velocity deviations. The fluctuations in these delta-velocity time histories are due primarily to the fluctuating character of the WSMR velocity estimates as shown in figures 10(c) and (d). These anomalies do not, however, detract from the usefulness of these curves since the general trends are clear. These curves indicate that, up to about 50 seconds, the free inertial velocities were varying randomly about zero error, but by 60 seconds, a definite offset was clear. This error continued to increase slowly to the end of the run. The RAINPAL run, on the other hand, quickly reduced the data-start errors, but there was no distinct improvement over the free inertial run until about 60 seconds. Following that time, the RAINPAL delta-velocity errors appear to slowly oscillate about zero throughout the remainder of the run.

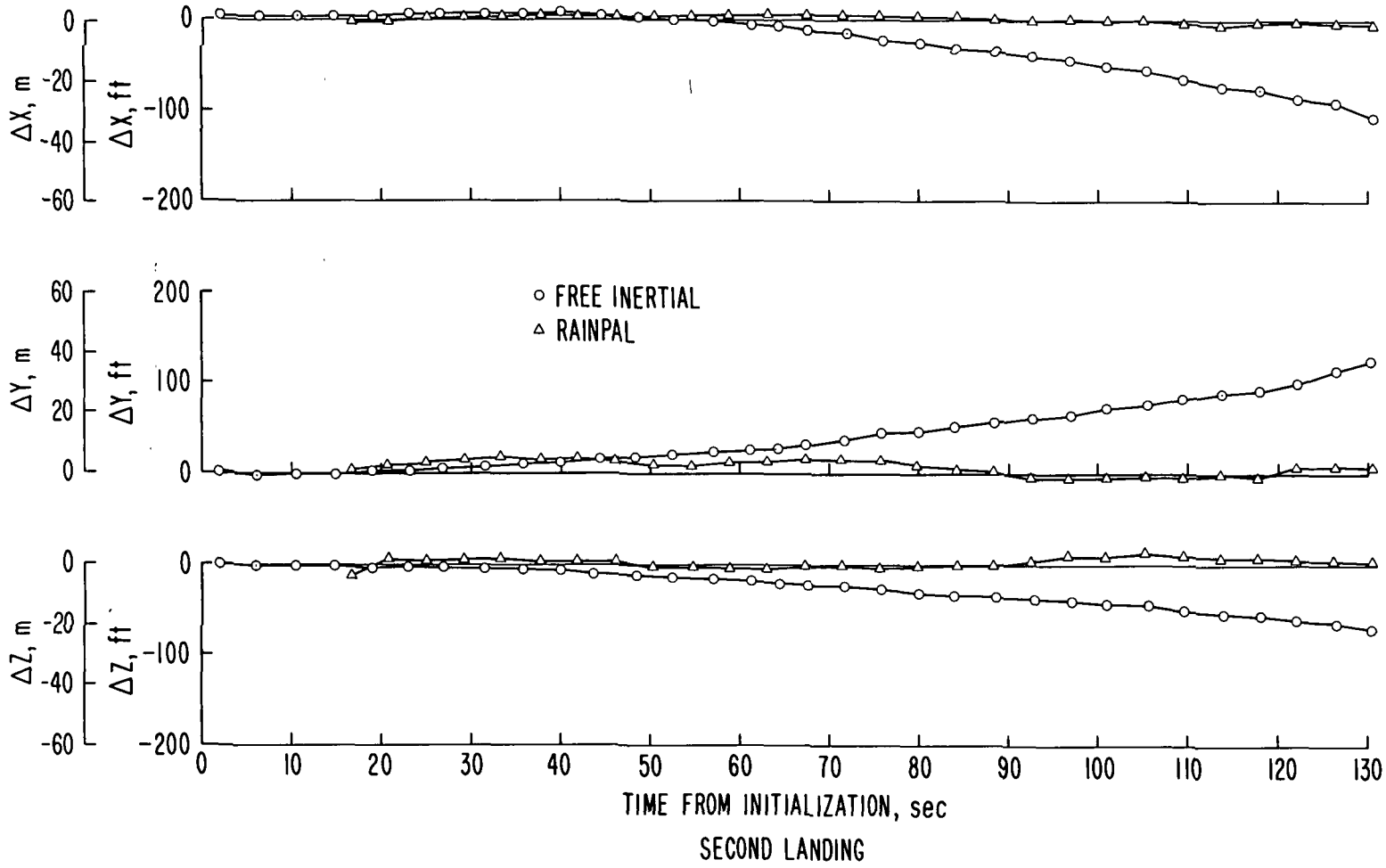

(a) ΔX, ΔY, ΔZ position deviations.

Figure 12.– Comparisons of navigation performance for free inertial and RAINPAL.

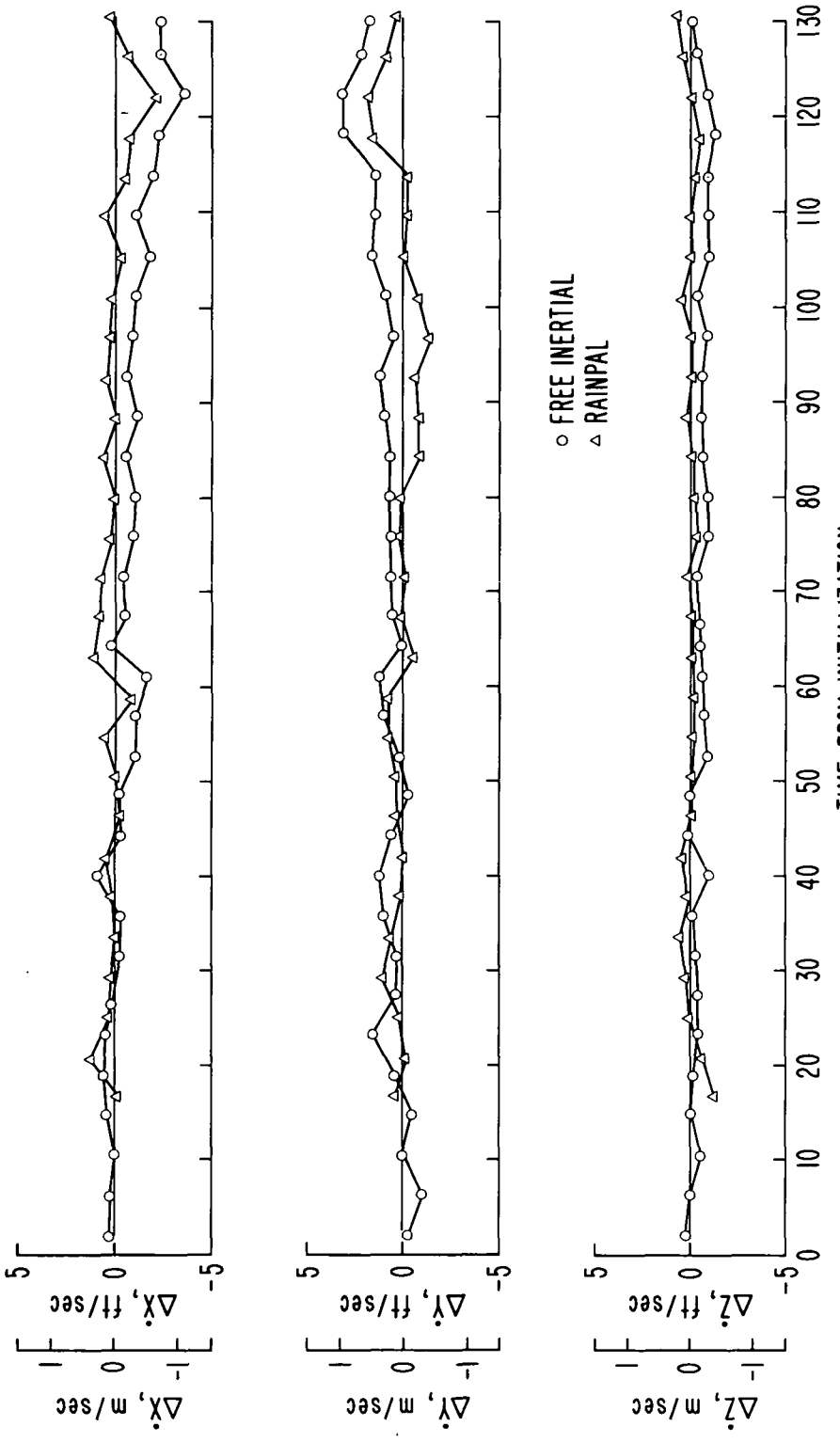

(b) $\Delta\dot{X}$, $\Delta\dot{Y}$, $\Delta\dot{Z}$ velocity deviations.

Figure 12.– Concluded.

Table 5 summarizes the deviations from the WSMR estimates of both the free inertial and RAINPAL run at 130 seconds. These data show that, during a final approach lasting only 130 seconds, free inertial navigation drift would result in unacceptable touchdown errors. The use of aiding, on the other hand, produced position estimates that were reduced an order of magnitude over the free inertial results. In velocity, the improvement factor is clouded by the random fluctuations in the WSMR estimates but appears to be about 2. The difficulty of determining improvement is partially overcome by the column of differences in Table 5. These differences are independent of the WSMR estimates and indicate quantitatively the improvement in navigation performance.

TABLE 5. – FREE INERTIAL, RAINPAL DEVIATIONS AT 130 SECONDS

Component	Free inertial	RAINPAL	Differences (free inertial – RAINPAL)
X	-31.8 m (-104 ft)	-1.83 m (-6 ft)	-30.0 m (-98 ft)
Y	37.2 m (122 ft)	1.52 m (5 ft)	35.7 m (117 ft)
Z	-21.3 m (-70 ft)	.61 m (2 ft)	-21.9 m (-72 ft)
$\dot{X}$	-.73 m/sec (-2.4 ft/sec)	.00 m (0.0 ft/sec)	-.73 m/sec (-2.4 ft/sec)
$\dot{Y}$	.52 m/sec (1.7 ft/sec)	.92 m/sec) (0.3 ft/sec)	-.40 m/sec (-1.3 ft/sec)
$\dot{Z}$	-.076 m/sec (-0.25 ft/sec)	.152 m/sec (0.5 ft/sec)	-.23 m/sec (-.075 ft/sec)

Figure 12 shows that the free inertial performance of the experimental inertial system operating in the runway coordinate system is at least equal to that of the commercial LTN-51 but, for the final approach, the drift in the experimental system is sufficiently large that unacceptable touchdown errors result. When aided with external data, the overall RAINPAL navigation performance (following completion of the Kalman filter initialization phase) approaches the touchdown performance shown in figure 10 most of the time throughout the entire landing approach.

Comparison of flight and simulation results – During the development of the RAINPAL system, a fairly elaborate digital computer simulation was developed for use in determining the performance that could be expected of the system. A matter of considerable interest was whether the simulation was sufficiently realistic to reliably predict performance. To investigate this matter, the simulation program was used in its Monte Carlo mode to generate five estimated trajectories for an approach and landing trajectory and to generate the measurement sequence, with data noise statistics duplicating as nearly as practicable the actual WSMR situation. The five sample estimated trajectories differed only in that each utilized a measurement sequence corrupted by a different, statistically independent sequence of measurement noise. According to the theory of extreme statistics, the range of results thus obtained is on the average a little more than $\pm 1\ \sigma$ at each time point. This range thus represents the deviations from the actual trajectory within which approximately 2/3 of the estimated trajectories should lie.

To compare simulated and actual results, the upper and lower deviation Y and Z bounds determined from the Monte Carlo simulation were applied to the WSMR Y and Z estimates for the third landing. These form the shaded area shown in figure 13, on which the Y and Z components of the three RAINPAL estimated trajectories are also plotted (repeated from figs. 10(a) and (b). It is seen that about half the Y and 2/3 of the Z RAINPAL points fall within the shaded area. Although WSMR accuracy (1 σ) is no better than 1.1 m (3.5 ft) in Y and 0.5 m (1.5 ft) in Z, these results indicate a satisfactory degree of consistency between the simulated and actual RAINPAL performance for the specific situation investigated here.

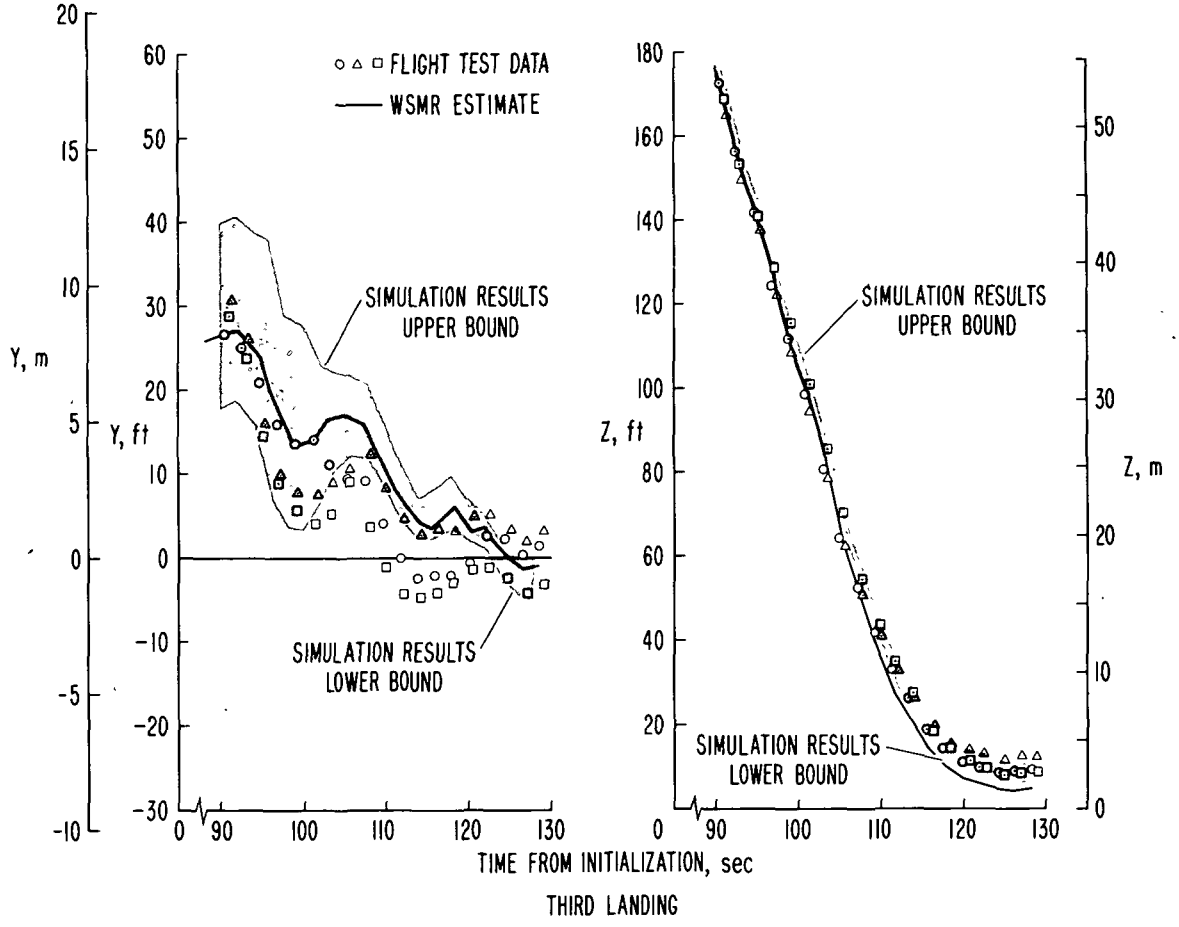

Figure 13. – Comparison of flight and simulation results.

Performance of the Kalman Filter Software

The square-root Kalman filter was programmed in fixed-point arithmetic for a XDS-920 digital computer. To minimize the computation time, the majority of the computer instructions was done in single precision. Once the filter had been debugged, its performance in the ground-based laboratory and in real time (ref. 7) was flawless without a single instance of anomalous behavior. This is significant because the square-root formulation of the Kalman filter has several important advantages over the more conventional formulations, particularly in an onboard application. In the past, lack of an efficient method to incorporate the modeling of random forcing functions has been a major deterrent to its use. The experience gained in these flight tests has demonstrated that this difficulty has been overcome.

RAINPAL APPLICATIONS

Aircraft Navigation

The present navigation accuracy requirements for automatic landing systems on commercial CTOL aircraft have not been established directly. Instead, the accuracy requirements are given in terms of total guidance, navigation, and control lateral and longitudinal dispersions. These dispersions (ref. 11) are for a category II automatic landing system on a runway 45.7 m (150 ft) wide and are normally expressed in terms of a two-standard deviation number, assuming the errors are normally distributed. On a one-standard deviation basis, the dispersion requirements are: longitudinal (X), 229 m (750 ft); and lateral (Y), 4.11 m (13.5 ft).

To arrive at a figure for the allowable standard deviation of the navigation error, a common method is to assume that equal error contributions are made by each system (guidance, navigation, and control) to the total. The total error, then, is the root-sum-square of the three equal contributors. On this basis, the allowable navigation error standard deviation is

$$X_{nav} = 132 \text{ m } (433 \text{ ft})$$

$$Y_{nav} = 2.38 \text{ m } (7.79 \text{ ft})$$

The allowable touchdown errors for the SSV are also given in terms of a standard deviation for the total guidance, navigation, and control errors. The current requirements are preliminary and, of necessity, very conservative, not only because the vehicle will touch down at high speed in any weather, but also because the vehicle is the first of its kind and, therefore, no historical data are available on which to base the allowable touchdown errors. The current total touchdown error standard deviations on a runway 45.7 m (150 ft) wide are

$$X = 73.15 \text{ m } (240.0 \text{ ft})$$

$$Y = 2.62 \text{ m } (8.6 \text{ ft})$$

$$Z = 4.62 \text{ m } (14.0 \text{ ft})$$

$$\dot{X} = 3.05 \text{ m/sec } (10 \text{ ft/sec})$$

$$\dot{Y} = 1.52 \text{ m/sec } (5 \text{ ft/sec})$$

$$\dot{Z} = 0.152 \text{ m/sec } (0.5 \text{ ft/sec})$$

Again, assuming that the total error is the root-sum-square of three equal contributors, the allowable navigation error contribution would be

$$X_{nav} = 42.23 \text{ m } (138.56 \text{ ft})$$

$$Y_{nav} = 1.51 \text{ m } (4.97 \text{ ft})$$

$$Z_{nav} = 2.46 \text{ m } (8.08 \text{ ft})$$

$$\dot{X}_{nav} = 1.76 \text{ m/sec } (5.77 \text{ ft/sec})$$

$$\dot{Y}_{nav} = 0.88 \text{ m/sec } (2.89 \text{ ft/sec})$$

$$\dot{Z}_{nav} = 0.088 \text{ m/sec } (0.289 \text{ ft/sec})$$

For other aircraft such as V/STOL, the automatic landing system dispersions are not established. However, the allowable dispersions probably will be similar to those of CTOL aircraft and certainly not more stringent than the present requirements of the SSV. Thus there seems to be little doubt that a navigation system meeting both the CTOL and SSV automatic landing system requirements would also meet those of a V/STOL aircraft.

A comparison is made in table 6 of the estimated standard deviation of the errors in the RAINPAL navigation system with the allowable navigation errors in an automatic landing system of a CTOL aircraft and the SSV. This table shows that a navigation system of the RAINPAL type, where aiding is provided by precision ranging system measurements and altimeter data, is fully capable of providing the navigation accuracy required for automatic landing of CTOL and V/STOL aircraft. It also appears that the accuracy would be adequate for the SSV automatic landing system with the possible exception of the vertical velocity requirement which seems overly stringent. Even so, had the accelerometer bias drift problem been discovered and resolved before the flight tests and had the ACPRS not experienced abnormal behavior along with excessive noise in the altimeter signals, there is reason to expect that the resulting improvement in the RAINPAL navigation performance over that presented here would have been adequate to satisfy the vertical velocity requirement.

Further applications of RAINPAL as a navigation system exist using navigation aids other than the precision ranging system. One outstanding advantage of the Kalman filter formulation is that other navigation aids operating singly or simultaneously can be easily included. Thus, the inclusion of such aids as VORTAC, TACAN, Instrument Landing System (ILS), or Microwave Landing System (MLS) is relatively simple. Indeed, simulation results (refs. 1-3) indicate that a system using VORTAC or TACAN aiding for enroute navigation and MLS aiding for terminal navigation would

have navigation accuracies during the landing approach comparable to those obtained with a precision ranging system. The use of the conventional ILS for aiding was shown in these studies to be less accurate but worthy of future study.

TABLE 6. – COMPARISON OF RAINPAL NAVIGATION ERRORS WITH ALLOWABLE ERRORS FOR CTOL AND SSV

Component	RAINPAL navigation error standard deviations	Navigation errors allowable for CTOL automatic landing systems	Navigation errors allowable for the SSV autoland system
X	0.9 ±0.6 m (3 ±2 ft)	132 m (433 ft)	43.2 m (139 ft)
Y	1.2 ±0.6 m (4 ±2 ft)	2.38 m (7.79 ft)	1.51 m (4.97 ft)
Z	0.9 ±0.6 m (3 ±2 ft)		2.46 m (8.08 ft)
$\dot{X}$	0.15 ±0.06 m/sec (0.5 ±0.2 ft/sec)		1.76 m/sec (5.77 ft/sec)
$\dot{Y}$	0.3 ±0.15 m/sec (1 ±0.5 ft/sec)		0.88 m/sec (2.89 ft/sec)
$\dot{Z}$	0.15 ±0.06 m/sec (0.5 ±0.2 ft/sec)		0.088 m/sec (0.289 ft/sec)

Independent Reference System

The WSMR cinetheodolite system is an independent reference system capable of providing an independent estimate of the trajectory of a vehicle. At present, WSMR is one of the best sources of independent data available and its value for this purpose, in most cases, is unquestioned.

The flight-test results presented here indicate that the RAINPAL system can provide accuracies comparable to those of WSMR, with RAINPAL being superior with regard to velocity determination due to the use of accelerometer data. The RAINPAL system also appears to have an advantage with regard to bias errors in the altitude estimates. As a result, it qualifies as an independent reference system that could replace the cinetheodolite system for applications where it is feasible to install the reference system onboard the test vehicle.

A major advantage of the RAINPAL approach for range instrumentation is that position and velocity estimates can be easily produced and printed out onboard in real time for immediate comparison with the system under test, with little or no dependence on postflight data processing. A further advantage is the greater operational flexibility of a RAINPAL type system in that (1) it can be used night or day and in adverse weather conditions, thus increasing available range time, (2) no human operators are needed for the transponders, (3) no synchronization or communication network is required, and (4) the ground transponders are lightweight and inexpensive compared to cinetheodolites.

CONCLUSIONS

The WSMR flight-test results represent an important step in demonstrating the feasibility of an aided inertial navigation system in which a Kalman filter is used to derive corrections to the inertial state by processing data from external sources. In these tests, the data processed were from a precision ranging system and from barometric and radar altimeters. As a result of analysis of the flight-test data presented in the text and observations regarding the operation of the computer software, the following conclusions were reached.

(1) The WSMR cinetheodolite system is one of the best sources of data presently available for providing an independent trajectory estimation. However, in this instance, there is evidence that the accuracy of the WSMR system is of the same order as that of RAINPAL. As a result, the WSMR tests could provide only an order-of-magnitude assessment of the RAINPAL performance. Estimates of this performance capability at touchdown, based on the evaluation of the data analysis described in this report, are presented in table 7 in terms of an estimated standard deviation of the navigation error.

TABLE 7. – STANDARD DEVIATION OF THE NAVIGATION ERROR AT TOUCHDOWN

Component	Standard deviation
X	0.9 ±0.6 m (3 ±2 ft)
Y	1.2 ±0.6 m (4 ±2 ft)
Z	0.9 ±0.6 m (3 ±2 ft)
$\dot{X}$	0.15 ±0.06 m/sec (0.5 ±0.2 ft/sec)
$\dot{Y}$	0.3 ±0.15 m/sec (1 ±0.5 ft/sec)
$\dot{Z}$	0.15 ±0.06 m/sec (0.5 ±0.2 ft/sec)

(2) Aided inertial systems of the RAINPAL type using precision range system data can provide navigation accuracies suitable for automatic landing of V/STOL and CTOL aircraft. The navigation performance of such a system would also meet the current requirements for the SSV.

(3) The RAINPAL system could be operated as an independent reference against which other navigation systems could be evaluated. Using a hardware improved ACPRS or a modern version of this system, the RAINPAL system should produce more accurate position and velocity estimates than the WSMR cinetheodolite system.

(4) One of the more significant conclusions resulting from the flight tests was that an effective square-root form of the Kalman filter has been demonstrated. This form incorporates an efficient method of handling random forcing functions and overcomes a major problem with many Kalman filter implementations in the past.

(5) The data-start procedure used to initialize the Kalman filter without prior knowledge of position or velocity (using only external measurement data) proved reliable and sufficiently accurate that rapid filter convergence to small estimation errors always occurred.

(6) The "free inertial" performance of the experimental inertial portion of the system operating in a runway coordinate system was shown to be at least equal to that of the commercial LTN-51 inertial navigation system. Subsequent hardware improvements and flight tests indicate that the performance has been much improved over that shown here. Even so, the present results show that, when aided with external precision range system measurements, the RAINPAL performance (after the Kalman filter initialization phase is completed) approaches the touchdown performance shown in fig. 10 a majority of the time throughout the entire landing approach.

(7) Use of the Kalman filter to estimate the barometric altimeter bias is an effective method for removing transients in the vertical (Z) position estimate which results from overflying ACPRS transponders and also from switching the filter data source from barometric to radar altimeter. Since the transients occurred at low altitude, barometric altimeter bias estimation would be an important consideration when all-weather landing operations are involved.

(8) Based on a limited number of simulation runs, the simulation program developed in support of the RAINPAL program and reported in references 1 and 2 produces results consistent with the flight results to a satisfactory degree.

Ames Research Center
National Aeronautics and Space Administration
Moffett Field, Calif., 94035, April 17, 1973

REFERENCES

1. McGee, L. A.; et al.: Navigation for Space Shuttle Approach and Landing Using an Inertial Navigation System Augmented by Data from a Precision Ranging System or a Microwave Scan Beam Landing Guidance System. NASA TM X-62, 123, 1970.

2. McGee, L. A., et al.: Navigation for Space Shuttle Approach and Landing Using an Inertial Navigation System Augmented by Various Data Sources, NASA TM X-58, 063, Vol. 1, p. 221, 1971.

3. Widnall, William S.; and Morth, H. R.: Space Shuttle Landing Navigation Using Precision Distance-Measuring Equipment. Final Rept., NASA CR-115, 138, 1971.

4. Schmidt, S. F.; Weinberg, J. D.; and Lukesh, J. S.: Application of Kalman Filtering to the C-5 Guidance and Control System, Theory and Applications of Kalman Filtering. AGARDograph 139, Feb. 1970.

5. Kaminski, Paul G.; Bryson, Arthur E.; and Schmidt, Stanley F.: Discrete Square Root Filtering: A Survey of Current Techniques, IEEE Trans. Automatic Control, Vol. AC-16, No. 6, Dec. 1971, pp. 727-736.

6. Schmidt, S. F.: Computational Techniques in Kalman Filtering, Theory and Applications of Kalman Filtering. AGARDograph 139, Feb. 1970.

7. Schmidt, S. F.: Precision Navigation for Approach and Landing Operations. Proceedings of the 1972 Joint Automatic Control Conference of the American Automatic Control Council, Stanford, Ca., Aug. 16-18, 1972, pp. 455-463.

8. Robinson, G. G.; and Bondi, M. J.: An Algorithm for Digital Resolution of Range for V/STOL Aircraft. NASA TN D-6232, 1971.

9. Schmidt, S. F.: Analysis and Modeling of Measurement Errors in the Ames Cubic Precision Ranging System, Rept. 72-30, Analytical Mechanics Associates, Inc., July 1972.

10. Goode, John E.: Cinetheodolite Error Statistics, Tech. Memorandum, Computing and Software, Inc., Feb. 1968.

11. Anon.: Advisory Circular AC No. 20-57A, Subject: Automatic Landing System (ALS), 12. Federal Aviation Administration, Dept. of Transportation, Jan. 1971.

NASA-Langley, 1973 — 21 A-4584

"The aeronautical and space activities of the United States shall be conducted so as to contribute . . . to the expansion of human knowledge of phenomena in the atmosphere and space. The Administration shall provide for the widest practicable and appropriate dissemination of information concerning its activities and the results thereof."

—NATIONAL AERONAUTICS AND SPACE ACT OF 1958

NASA SCIENTIFIC AND TECHNICAL PUBLICATIONS

TECHNICAL REPORTS: Scientific and technical information considered important, complete, and a lasting contribution to existing knowledge.

TECHNICAL NOTES: Information less broad in scope but nevertheless of importance as a contribution to existing knowledge.

TECHNICAL MEMORANDUMS: Information receiving limited distribution because of preliminary data, security classification, or other reasons. Also includes conference proceedings with either limited or unlimited distribution.

CONTRACTOR REPORTS: Scientific and technical information generated under a NASA contract or grant and considered an important contribution to existing knowledge.

TECHNICAL TRANSLATIONS: Information published in a foreign language considered to merit NASA distribution in English.

SPECIAL PUBLICATIONS: Information derived from or of value to NASA activities. Publications include final reports of major projects, monographs, data compilations, handbooks, sourcebooks, and special bibliographies.

TECHNOLOGY UTILIZATION PUBLICATIONS: Information on technology used by NASA that may be of particular interest in commercial and other non-aerospace applications. Publications include Tech Briefs, Technology Utilization Reports and Technology Surveys.

Details on the availability of these publications may be obtained from:

SCIENTIFIC AND TECHNICAL INFORMATION OFFICE

NATIONAL AERONAUTICS AND SPACE ADMINISTRATION

Washington, D.C. 20546